Geosci. Model Dev. Discuss., 7, 1063–1114, 2014
www.geosci-model-dev-discuss.net/7/1063/2014/
doi:10.5194/gmdd-7-1063-2014

Geoscientific Model Development Discussions
Open Access

Development of the Surface Urban Energy and Water balance Scheme (SUEWS) for cold climate cities

L. Järvi[1], C. S. B. Grimmond[2,3], M. Taka[4], A. Nordbo[1], H. Setälä[5], and I. B. Strachan[6]

[1]University of Helsinki, Department of Physics, Helsinki, Finland
[2]King's College London, Department of Geography, London, UK
[3]University of Reading, Department of Meteorology, Reading, UK
[4]University of Helsinki, Department of Geosciences and Geography, Helsinki, Finland
[5]University of Helsinki, Department of Environmental Sciences, Helsinki, Finland
[6]McGill University, Department of Natural Resource Sciences, QC, Montreal, Canada

Received: 11 November 2013 – Accepted: 16 January 2014 – Published: 27 January 2014

Correspondence to: L. Järvi (leena.jarvi@helsinki.fi)

Published by Copernicus Publications on behalf of the European Geosciences Union.

Abstract

The Surface Urban Energy and Water balance Scheme (SUEWS) is developed to include snow. The processes addressed include accumulation of snow on the different urban surface types; snow albedo and density aging; snow melting and re-freezing of melt water. Individual model parameters are assessed and independently evaluated using long-term observations in two cold climate cities, Helsinki and Montreal. Eddy covariance sensible and latent heat fluxes and snow depth observations are available for two sites in Montreal and one in Helsinki. Surface runoff from two catchments (24 and 45 ha) in Helsinki and snow properties (albedo and density) from two sites in Montreal are also analysed. As multiple observation sites with different land-cover characteristics are available in both cities, model development is conducted independently of evaluation.

The developed model simulates snowmelt related runoff well (within 10 % and 6 % for the two catchments in Helsinki when there is snow on the ground), with the springtime peak estimated correctly. However, the observed runoff peaks tend to be smoother than the simulated ones, likely due to the water holding capacity of the catchments and the missing time lag between the catchment and the observation point in the model. At all three sites the model simulates snow accumulation and melt events well, but underestimates snow depth by 18–20 % in Helsinki and 29–33 % in Montreal. The model is able to reproduce the diurnal pattern of net radiation and turbulent fluxes of sensible and latent heat during cold snow, melting snow and snow free periods. Largest model uncertainties are related to the melting period. The results show that the enhanced model can correctly simulate the exchange of energy and water in cold climate cities, and is appropriate to be nested in a larger scale atmospheric model or used independently for urban planning.

GMDD
7, 1063–1114, 2014

1 Introduction

Today more than half of world's population resides in urban areas, and this fraction is expected to increase in the next decades (Martine and Marshall, 2007). Thus the ability to understand and forecast the urban climate is crucial for sustainable urban planning and our quality of life. The exchanges of heat and water between the surface and the atmosphere are of great importance to urban climate studies. These exchanges describe the surface forcing in numerical weather prediction, air quality and climate models, and thus their correct simulation is highly important. In urban areas several land surface models, with different complexity, simulate these energy exchanges, but none of the models outperforms the others (Grimmond et al., 2011). The latent heat flux is commonly underestimated and sometimes even ignored, which increases the direct heat emissions to the atmosphere. Furthermore, most of these models only concentrate on the surface-atmosphere interactions without any connections to the water cycles in urban areas. Similarly, several hydrological models to simulate urban drainage and the surface runoff in urban areas have been developed (Mitchell et al., 2003, 2008; Easton et al., 2007; Jacobson, 2011), but these do not typically consider the full energy balance.

Both in land surface and hydrological model studies, urban areas located in cold climates have been little studied despite their particular sensitivity to regional and global climate change. Thus appropriate, robust, well tested modeling tools are needed. Modeling studies of cold cities are focused on a few sites mainly in North-America (e.g. Valeo and Ho, 2004; Lemonsu et al., 2010; Leroyer et al., 2010) and Scandinavia (e.g. Semádeni-Davies et al., 1998). These emphasize the need for correct description of snow cover in hydrological models. Snow affects surface energy partitioning via albedo and snowmelt, re-freezing and the phase change related energy fluxes. The energy required for snow melt can be of the same magnitude as the sensible and latent heat fluxes (Lemonsu et al., 2010). Snow impacts water availability and its melt may cause springtime floods in urban areas (Semádeni-Davies and Bengtsson, 1998). To keep

GMDD
7, 1063–1114, 2014

cities operational, snow is often redistributed within neighborhoods and/or is transported away (Semádeni-Davies and Bengtsson, 1998, 1999), which impacts both the energy and water cycles.

The lack of observational data in urban areas with continuous winter snow cover make the determination of model parameters and flux evaluation challenging. Surface-atmosphere exchange of sensible and latent heat can be measured directly using the eddy covariance technique, but these observations are relatively rare especially in cold climate cities. Notable exceptions include the work of Lemonsu et al. (2008); Vesala et al. (2008); Bergeron and Strachan (2012); Nordbo et al. (2012a, b). These studies have found a strong seasonality in the energy exchanges and a need for correct estimation of anthropogenic heat emissions from building sources, notably heating in winter. Similarly, the few hydrological studies have shown strong seasonality in stormwater runoff and differences in the amount of the snow melt when compared to natural environments (Bengtsson and Westerström, 1992; Semádeni-Davies and Bengtsson, 1998; Valtanen et al., 2013).

The purpose of this study is to develop a model that can correctly simulate both the energy and water balances in cold climate cities. The model developed is included in the Surface Urban Energy and Water balance Scheme (SUEWS, Järvi et al., 2011) with particular attention to the accumulation and melting of snow. The development and independent evaluation of the model uses several years of data collected in Helsinki (60° N, 24° W) and Montreal (45° N, 73° W). These include turbulent fluxes of heat and water measured with the eddy covariance technique, stormwater runoff and snow properties.

2 Methods

2.1 The Surface Urban Energy and Water balance Scheme (SUEWS)

The Surface Urban Energy and Water balance Scheme SUEWS (Järvi et al., 2011) simulates the urban energy and water balance components from local or neighborhood scale using hourly meteorological forcing data. These data inputs are kept to a minimum to enhance the flexibility of the model and commonly include: measured solar radiation (probably least frequently measured), air temperature, relative humidity, surface air pressure, wind speed and precipitation. In addition, it requires information about the characteristics of the area to be simulated, such as surface cover fractions of paved, buildings, evergreen trees/shrubs, deciduous trees/shrubs, irrigated grass, non-irrigated grass and water, and population density and building and tree heights.

Rates of evaporation-interception for a single layer for each of the surface types are calculated and below each surface type, except water, there is a single soil layer. At each time step (5 min to 1 h) the moisture state of each surface and soil type is calculated. Horizontal water movements at the surface and in the soil are incorporated. Latent heat flux is calculated with a modified Penman–Monteith equation and sensible heat flux as a residual from the available energy minus the latent heat. The model contains several sub-models, for example for net all-wave radiation (NARP, Offerle et al., 2003; Loridan et al., 2011), storage heat fluxes (Grimmond et al., 1991), anthropogenic heat fluxes, and external irrigation.

2.1.1 New developments

The new version of SUEWS presented here incorporates a parameterization for snow cover. Previously, snow cover was a required input that was assumed to cover the whole grid area and only directly impacted the radiation. Now, accumulation and melting of snow are estimated, with impact to net all-wave radiation, evaporation, and other water balance components. For each surface type, the energy and water balances are

GMDD
7, 1063–1114, 2014

calculated separately for snow-free and snow-covered areas and the model outputs are weighted according to their respective fractions. The energy and water flow calculations in the snow free surface types follow those in the original version of the model (Järvi et al., 2011). Here we present the equations related to the snow covered surface which is treated as a single snow layer.

The energy balance of the snow covered surface modified for urban areas can be written as (e.g. Oke, 1987; Cline, 1997)

$$Q_M + \Delta Q_{S,I} = Q^* - Q_H - Q_E + Q_P - Q_g + \Delta Q_A \quad (\mathrm{W\,m^{-2}}) \tag{1}$$

where Q_M is the latent heat storage change caused by melting or freezing, $\Delta Q_{S,I}$ is the change in the storage heat of the snow, Q^* is the net all-wave radiation, Q_H and Q_E are the turbulent sensible and latent heat fluxes, Q_P is the heat released by liquid precipitation on snow, Q_g is the heat exchange between the snow and the soil below and ΔQ_A is the net advective heat flux. Snow melt occurs if the net energy input to the snow is positive (i.e. right-hand side of the Eq. (1) > 0). The advective heat flux Q_A and the ground heat flux Q_g are assumed to be negligible relative to the other terms so they are not calculated (e.g. Lemonsu et al., 2010).

The link to the snow mass balance is through Q_E or evaporation (E):

$$P + F = E + R + T_R + \Delta S_{WE} \quad (\mathrm{mm\,h^{-1}}) \tag{2}$$

where P is precipitation (snowfall, rain), F is liquid water that freezes on a snow-free surface, R is the runoff from the snowpack, T_R is the transport of snow from the study area (e.g. via snow-clearing) and ΔS_{WE} is the change in (liquid and solid phase) snow water equivalent (S_{WE}).

2.1.2 Surface albedo

Snow affects Q^* by modifying the albedo of the surface and thus the reflected shortwave radiation, and the upwelling long wave radiation as the surface temperature of snow and snow free surface are different. The snow albedo (α_s) varies with snow age for each time step (Δt), based on whether it is the "cold snow period" when melting does not occur (Baker et al., 1990; Lemonsu et al., 2010):

$$\alpha_s(t+\Delta t) = \alpha_s(t) - \tau_a \frac{\Delta t}{\tau_d} \tag{3}$$

or the "warm snow period" when snow melt occurs (Verseghy, 1991; Lemonsu et al., 2010):

$$\alpha_s(t+\Delta t) = \left[\alpha_s(t) - \alpha_s^{min}\right] \exp(-\tau_f \frac{\Delta t}{\tau_d}) + \alpha_s^{min} \tag{4}$$

For simplicity, the warm snow period is defined as times when air temperature (T_a) is above 0 °C. α_s^{min} is the minimum snow albedo, τ_d is a period of one day (86 400 s), and τ_a and τ_f are time constants related to the snow aging. After new snowfall, when S_{WE} exceeds 2 mm, the snow albedo is reset to its maximum (fresh snow) value (α_s^{max}, Koivusalo and Kokkonen, 2002). The upward long-wave radiation uses a constant snow emissivity.

2.1.3 Snow heat storage

The net heat storage in the snow can be considered to describe the convergence or divergence of sensible heat fluxes within the snowpack volume. This is calculated using the objective hysteresis model (OHM; Grimmond et al., 1991):

$$\Delta Q_{S,l} = a_1 Q^* + a_2 \frac{\Delta Q^*}{\Delta t} + a_3 \tag{5}$$

where a_1, a_2 and a_3 parameters are set by the model user. The first term describes the direct heating by radiation, the second term the hysteresis of the warming and cooling phases, and the third the time lag. $\Delta Q_{S,l}$ is negative when the snowpack loses energy

GMDD
7, 1063–1114, 2014

and the snowpack cools increasing the "cold content" of the snow (energy needed to heat the snow to 0 °C), and positive when the snow is heated towards 0 °C and the cold content is filled. Cold content is the total energy needed before the melting of snow can start (Bengtsson, 1982).

2.1.4 Energy for melting and freezing

There are two main approaches to estimate the snowmelt and refreezing of the melt water (M) and the related energy (e.g. Martinec, 1989; Tobin et al., 2013): (1) the energy balance method, where M is calculated as a residual from the other energy balance components, and (2) the degree day method where M is calculated using daily or hourly air temperatures and possibly solar radiation. Although the first is more physically-based it requires more input variables, whereas the latter uses more readily available variables. Comparisons of the two methods have found insignificant differences in the calculated melted water (Kustas et al., 1994; Debele et al., 2010). However, the site specific degree day parameters need to be assessed (Bengtsson, 1984).

In SUEWS the second approach is used via a radiation-temperature index for each surface type i (Kustas et al., 1994; Semadeni-Davies et al., 2001; Tobin et al., 2013). Snowmelt induced runoff is delayed by re-freezing of melted water (Bengtsson, 1982), particularly in spring, when the diurnal variations in air and snow surface temperatures are large. Daytime melt-water refreezes after sunset, releasing energy. Traditionally, the degree-day methods have utilized a daily time step, but in urban areas this has poor performance (Bengtsson, 1984). Therefore an hourly time step is utilized here. Melting and freezing occurs as a function of air temperature (T_a) and Q^* under three conditions:

$$M_i = \begin{cases} a_\mathrm{r} Q^* & Q^* > 0\,\mathrm{W\,m^{-2}},\ T_\mathrm{a} \geq 0\,^\circ\mathrm{C} \\ a_\mathrm{t} T_\mathrm{a} & Q^* < 0\,\mathrm{W\,m^{-2}},\ T_\mathrm{a} \geq 0\,^\circ\mathrm{C} \\ a_\mathrm{f} T_\mathrm{a} & T_\mathrm{a} < 0\,^\circ\mathrm{C} \end{cases} \tag{6}$$

with factors for radiation melt a_r (mm W^{-1} h^{-1}), temperature melt a_t and freeze a_f (mm °C^{-1} h^{-1}) which are typically linearly related with $a_f \le a_t$ (Tobin et al., 2013). M_i cannot be larger than the amount of solid snow in the pack and the amount of freezing water cannot exceed the amount of liquid water in the snow. The energy consumed in melting and re-freezing is

$$Q_{M,i} = \rho_w M_i L_f \tag{7}$$

where ρ_w is the liquid water density at 0 °C (kg m^{-3}) and L_f is the latent heat of fusion at 0 °C (J kg^{-1}).

Besides re-freezing of melted water, the snowmelt runoff from the snowpack is delayed by the amount of liquid water the snow can hold (Bengtsson, 1982; Semádeni-Davies and Bengtsson, 1998). In SUEWS, this liquid water retention capacity (C^R) is calculated as a function of snow density (ρ_s, kg m^{-3}) (Anderson, 1976; Jin et al., 1999):

$$C_i^R = \begin{cases} C_{\min}^R, & \rho_s \ge \rho_e \\ C_{\min}^R + \left(C_{\max}^R - C_{\min}^R\right) \frac{\rho_s - \rho_e}{\rho_s}, & \rho_s < \rho_e \end{cases} \quad \text{(in kg kg}^{-1}\text{)} \tag{8}$$

where $C_{\min}^R$ and $C_{\max}^R$ are the minimum and maximum capacities and ρ_e is a threshold density set to 200 kg m^{-3}. With time, the snow density changes (Verseghy, 1991):

$$\rho_s(t + \Delta t) = \left[\rho_s(t) - \rho_s^{\max}\right] \exp\left(-\frac{\tau_r \Delta t}{\tau_h}\right) + \rho_s^{\max} \tag{9}$$

to a maximum snow density $\rho_s^{\max}$ with a time constant τ_r. τ_h is the seconds in an hour (3600 s h^{-1}). After snowfall, ρ_s is calculated as the weighted average of the fresh ($\rho_s^{\min}$) and previous snow densities.

GMDD
7, 1063–1114, 2014

2.1.5 Heat release by rain on snow

A rain on snow event provides heat, when the precipitation temperature is above the liquid/solid threshold (T_{lim}) (Sun et al., 1999):

$$Q_{P,i} = \rho_\text{w} c_\text{w} P_i (T_\text{a} - T_{\text{lim}}), \tag{10}$$

where c_w is the specific heat capacity of water (J kg^{-1} K^{-1}), and P_i is the precipitation on ith surface (in m s^{-1}). Here, it is assumed that the temperature of the precipitation is at the air temperature (Sun et al., 1999). Rain stays as a liquid and is routed to melt water store.

2.1.6 Latent heat flux and evaporation

To calculate the latent heat flux (Q_E) a modified Penman–Monteith equation is used with a negligible surface resistance for the snow covered surfaces and an available energy that is constrained by snowmelt and re-freezing of the melt water:

$$Q_{\text{E},i} = \frac{s(Q_\text{P} - Q_{\text{M},i}) + \frac{c_p \rho V}{r_\text{a}}}{s + \gamma}, \tag{11}$$

where s is the slope of the saturation vapour pressure curve over ice (Pa °C^{-1}) calculated according to Lowe (1977), γ in the psychometric constant (Pa °C^{-1}), c_p is the heat capacity of air (J kg^{-1} K^{-1}), ρ is the density of air (kg m^{-3}), V is the vapour pressure deficit (Pa) and r_a is the aerodynamic resistance (s m^{-1}). To calculate the snow surface r_a, the roughness length for heat and water vapour ($z_{0\text{v}}$, m) is calculated using (Voogt and Grimmond, 2000):

$$z_{0\text{v}} = z_{0\text{m}} \exp(-20), \tag{12}$$

where $z_{0\text{m}}$ is the roughness length for momentum (m).

2.1.7 Change in snow water equivalent

For the water mass balance calculations, the model adopts a 5 min time step in order to respond to precipitation and snowmelt events. When the surface is completely covered by snow, the snow water equivalent of the ith surface type ($S_{\mathrm{WE},i}$) is calculated:

$$S_{\mathrm{WE},i}(t+\Delta t) = S_{\mathrm{WE},i}(t) + (P_i + F_i - E_i - R_i - T_{R,i}). \quad (\text{in mm } (5\,\text{min})^{-1}) \tag{13}$$

If melt occurs ($M_i > 0$) the water is held in the snowpack until the liquid water holding capacity C_i^R is exceeded. The excess water goes directly to runoff (R_i). If the surface is partially covered with snow, the excess water is added to the snow free surface storage (S_i) and so follows the snow free surface equations (Järvi et al., 2011). If a negative $S_{\mathrm{WE},i}$ occurs, the calculated evaporation is assumed to be too large and is reduced by equivalent amount (constrained by E_i).

People are assumed to clear and/or transport snow from paved and built surfaces ($T_{R,i}$) when a threshold value of the $S_{\mathrm{WE,Lim}}$ is exceeded. This behaviour is neighbourhood specific (e.g. city or neighbourhood ordinances, snow clearance priorities). The S_{WE} is assumed to be reduced to the $S_{\mathrm{WE,Lim}}$ at the next site specific snow clearing time period.

The snowpack starts to form when the surface temperature $T_\mathrm{s} < 0\,^\circ\mathrm{C}$ and under two conditions: when solid precipitation occurs and/or when water on a snow free surface freezes (F_i). The snow depth s_d (mm) is:

$$s_{\mathrm{d},i} = S_{\mathrm{WE},i}\frac{\rho_\mathrm{w}}{\rho_\mathrm{s}}. \tag{14}$$

2.1.8 Surface fraction of snow

One of the most important factors controlling the energy balance and snowmelt is the patchiness of snow (Swenson and Lawrence, 2012). This is particularly important in urban areas, where snow clearing from streets and roofs takes place regularly (Semádeni-Davies, 1999). During the melt period, surface type specific depletion curves are used to approximate the fraction of snow cover (f_s) as a function of S_{WE} (e.g. Ek et al., 2003; Valeo and Ho, 2004). These are a function of surface specific maximum snow water equivalent S_{WE}^{max} that control the initiation of snow patchiness (Swenson and Lawrence, 2012). For vegetated surfaces, the Ek et al. (2003) form of the function is used with coefficients derived from Swenson and Lawrence's (2012) data:

$$f_{s,veg} = 1 - \left(\frac{1}{\pi}\text{acos}\left(2\frac{S_{WE,veg}}{S_{WE,veg}^{max}} - 1\right)\right)^{1.3} \tag{15a}$$

For paved and built surfaces, the equations were derived from Valeo and Ho's (2004) data:

$$f_{s,pav} = \left(\frac{S_{WE}}{S_{WE,pav}^{max}}\right)^2 \tag{15b}$$

$$f_{s,bldg} = 0.5\left(\frac{S_{WE}}{S_{WE,bldg}^{max}}\right) \quad \frac{S_{WE}}{S_{WE,bldg}^{max}} < 0.9$$

$$f_{s,bldg} = \left(\frac{S_{WE}}{S_{WE,bldg}^{max}}\right)^8 \quad \frac{S_{WE}}{S_{WE,bldg}^{max}} \geq 0.9 \tag{15c}$$

The different depletion curves between vegetation and impervious surfaces are used as human activities redistribute snow. For example, large roadside snow piles are created that melt slowly through the spring. In contrast, during the accumulation period snow is assumed to fall evenly on all surfaces.

2.1.9 Leaf area index

Changes in phenology, such as growing season length, vary from year to year. At high latitudes, air temperature is a good proxy for leaf growth in spring, whereas the leaf-off

GMDD
7, 1063–1114, 2014

is initiated by length of day (Keskitalo et al., 2005). However, air temperature influences the rate of leaf fall.

Daily leaf area index ($\mathrm{LAI}_{d,i}$) is calculated:

$$\mathrm{LAI}_{d,i} = \begin{cases} \mathrm{LAI}^{b1}_{d-1,i}\mathrm{GDD}\cdot c_1 + \mathrm{LAI}_{d-1}, & \text{leaf-on}, \; T_d > T_{\mathrm{BaseGDD}} \\ \mathrm{LAI}^{b2}_{d-1,i}\mathrm{SDD}\cdot c_2 + \mathrm{LAI}_{d-1}, & \text{leaf-off}, \; T_d < T_{\mathrm{BaseSDD}} \\ \mathrm{LAI}_{d-1,i}b_3(1-\mathrm{GDD})\cdot c_3 + \mathrm{LAI}_{d-1}, & \text{leaf-off}, \; t_d < 12\,\mathrm{h} \end{cases} \tag{16}$$

where GDD and SDD are the growing and senescence degree days, $b_{1,2,3}$ and $c_{1,2,3}$ control the rate of change in LAI and T_{BaseSDD} is the base temperature for senescence.

2.2 Measurement sites and measurements

The model is applied in two cities that typically have extended periods of snow coverage: Helsinki and Montreal. As multiple observation sites with different land-cover characteristics are available in both cities, model development is conducted independently of evaluation.

2.2.1 Helsinki, Finland

Meteorological and hydrological observations from three areas of Helsinki are used (Fig. 1). At the Kumpula (Ku, SMEAR III) site both meteorological forcing and evaluation data are measured (Järvi et al., 2009a). In addition, the observed runoff from Pasila (Pa) and Pihlajamäki (Pi) catchments are used for model development and evaluation. Ku is located 4 km north-east of the Helsinki city centre in a suburban area and 3.8 km from Pa and Pi (Fig. 1). Both Pa and the built sector of Ku (Ku1) have large areas of impervious surfaces (62 %). At both sites, the buildings are mostly office buildings with mean height of 15 m (Pa) and 11 m (Ku1). Pa has pedestrian areas at two heights with extensive concrete surfaces creating a complex morphology. The other two sectors around the SMEAR III flux tower (Ku2, Ku3) and the Pi catchment are more vegetated

GMDD
7, 1063–1114, 2014
Development of the SUEWS for cold climate cities
L. Järvi et al.

(Table 1). Pi, with 34 % impervious surfaces, is a typical suburban area in Helsinki with multi-family block houses.

Tower based eddy covariance (EC) sensible and latent heat fluxes measured at 31 m, with an ultrasonic anemometer (Metek, USA-1) and a closed-path infrared gas analyser (LI-7000, respectively, Li-COR Biosciences, Lincoln, NE, USA) at Ku are used. Post-processing of the 10 Hz data use commonly accepted procedures described in detail in Järvi et al. (2009b) and Nordbo et al. (2012a).

Tower top air temperature (platinum resistant thermometer, Pt-100, "*in-house*"), wind speed (Thies Clima 2.1x, Goettingen, Germany) and incoming and outgoing short- and long-wave radiation (CNR1, Kipp&Zonen, Delft, Netherlands) are used to force and test the model. Other forcing data measured on a nearby roof (24 m a.g.l.) include air pressure (Vaisala DPA500, Vaisala Oyj, Vantaa, Finland), relative humidity (Vaisala HMP243), and precipitation (rain gauge, Pluvio2, Ott Messtechnik GmbH, Germany). Snow depth measured next to the tower by the Finnish Meteorological Institute is used in the model evaluation.

Runoff was monitored at one minute intervals using a OCM Pro CF flow meter (Nivus GmbH, Eppingen, Germany) mounted in the two catchment storm flow discharge pipes from September 2010 to 30 April 2011 (see Table 2 for data availability). In Pi, excess pipe flow was observed causing runoff at unexpected times; because of the water quality observed, this is thought to be associated with pipe leakage in household water systems. From the beginning of September, the excess pipe flow was 0.0038 $m^3 s^{-1}$; it increased to 0.0125 $m^3 s^{-1}$ at the end of the measurement campaign. This pipe flow was removed from the analysis when assessing the runoff as pipe leakage is not modelled currently.

2.2.2 Montreal, Canada

Two residential areas with impervious cover of 71 % (RI, Rosemont–La-Petite-Patrie borough) and 49 % (Pr, Pierrefonds-Roxboro borough) 18 km apart were modelled (see Bergeron and Strachan (2012) for map). The more densely populated RI has two to three storey buildings whereas the suburban Pr is a single family house residential area (Table 1).

At both sites, a tower mounted (26 m a.g.l.) sonic anemometer (CSAT3, Campbell Scientific Canada Corp., Edmonton, AB, Canada) and an open-path infrared gas analyser (LI-7500, Li-COR Biosciences, Lincoln, NE, USA) provided the 20 Hz data that are post-processed to EC fluxes of sensible and latent heat (Bergeron and Strachan, 2012). Forcing data of air temperature and relative humidity (HMP45C-212 at Rl, HMP45C at Pr, Campbell Scientific Canada Corp.), pressure (Barometric pressure sensor, RM Young Model 61205V, RM Young Company, Michigan, USA) and radiation (CNR1) are from the EC tower at 25 m a.g.l. Snow depths were monitored in the backyard of Pr and on the roof at Rl with snow ranging sensors (SR5, Campbell Scientific Canada Corp.). Snow properties, including snow density and albedo, were regularly (weekly: 2007/08 winter or bi-monthly: 2008/09 winter) observed for undisturbed snow, sidewalks, lawns and rooftops. Observations from Coteau-du-Lac (35 km southwest from Pr) and Pierre Elliot Trudeau Airport data (7 km from Pr and 16 km from Rl) (National Climate Data and Information Archive of Canada, 2013) are used to create a precipitation dataset with snow/rain separation.

2.3 Model runs

In Helsinki, SUEWS was run for Ku for three years (January 2010 till December 2012) and for the two catchments for 16 months (January 2010–April 2011). At all three sites, the first seven months are a spin-up period for the model that is neither used in model development nor testing. The spin-up time allows the model to become independent of the initial conditions set by the user. Even in urban areas, soil moisture initial state has a large impact on urban land surface model performance (Best and Grimmond, 2013). The remainder of the periods are used for model development and evaluation. In Ku, data prior to 2012 are used to develop and adjust model parameters: Q^*, upward shortwave radiation, and upward and downward long wave radiation are used to adjust the snow, and surface albedo (Eqs. 3 and 4), and Q_H and Q_E to test the parameterizations for Q_M and $\Delta Q_{S,I}$ (Eqs. 5 and 6). The runoff measured in the more dense catchment (Pa) is used to constrain the temperature and radiation melt rates (Eq. 6), retention capacity of the snow (Eq. 8) and the limit for the liquid precipitation. Q^* and its components, Q_H and Q_E, the snow depth from Ku in 2012, and the runoff from the medium-intensity catchment are used to independently evaluate the model.

The meteorological data measured at the Ku site are used to force the model for all three sites. The data are gap filled using the procedures described in Järvi et al. (2012). Due to the very different characteristics surrounding the Kumpula tower, the model is run for the three surface cover areas within a 1 km radius circle. The flux time series evaluated against observations are combined from the surface cover areas (Ku1–3) based on the prevailing wind direction.

In Montreal, only the first month of the 22 months (December 2007 till September 2009) is used as a spin-up. The short spin-up time is chosen as we want to use two snow melt periods in model development and testing. The remainder of the suburban dataset (Q^*, Q_H, Q_E, snow depth, snow density and albedo) is used for the model development: snow density and albedo are used to determine shape of the snow aging curves (Eqs. 3, 4 and 9), the Q^* the surface and snow albedo, and Q_H, Q_E the other snow related parameterizations. The urban site observations are used for independent evaluation of the model. The model domain is a 1 km radius circle around the flux tower.

The results are analysed by considering snow-off, cold snow and melting snow periods. For snow-off, the simulated snow depth is zero, whereas the cold snow and melting snow periods are separated by the air temperature 0 °C.

2.4 Evaluation statistics

Several statistics are used to evaluate the model performance (e.g. Daley, 1991). Linear regression is used to describe the linear dependence between the independent variable, in our case the model output X_{Mod}, and the dependent variable, the observations (X_{Obs}). The slope (S) relative to 1 and intercept (I) relative to zero provide information on the model performance. Further, goodness of fit is evaluated using the root mean square error (RMSE):

$$\mathrm{RMSE} = \sqrt{\frac{\sum (X_{\mathrm{Mod}}(t) - X_{\mathrm{Obs}}(t))^2}{N}} \tag{17}$$

where N is the number of data points. Like the intercept in the linear regression, the RMSE has the units of the variables being evaluated and it depends on the magnitude of the mean variables. Therefore it is useful to normalize the RMSE (nRMSE) relative to the range of values observed:

$$\mathrm{nRMSE} = \frac{\mathrm{RMSE}}{X_{\mathrm{Obs,\,max}} - X_{\mathrm{Obs,\,min}}} \tag{18}$$

In addition, the mean biased error (MBE) between the modelled and observed time series is used:

$$\mathrm{MBE} = \sum (\bar{X}_{\mathrm{Mod}} - \bar{X}_{\mathrm{Obs}}), \tag{19}$$

where over bar means average. All RMSE, nRMSE and MBE would ideally be zero.

3 Results

3.1 General weather conditions

The weather conditions during the modelled period for Helsinki and Montreal are shown in Figs. 2 and 3, respectively. Daytime solar radiation experiences a strong seasonal pattern, with the 15° latitudinal difference causing more rapid changes and stronger amplitude in Helsinki than Montreal. In summer, $K\downarrow$ reaches 970 W m^{-2} in the latter, whereas in Helsinki the maxima remain below 830 W m^{-2}. In winter, the solar radiation in Helsinki is very low (< 120 W m^{-2}), whereas Montreal peaks are below 400 W m^{-2}.

GMDD
7, 1063–1114, 2014

Despite the difference in $K\downarrow$, air temperatures are fairly similar in both cities. Daily maxima mean temperatures are around 26 °C in summer, while the minimum daily mean temperature in winter in Helsinki is −20 °C and in Montreal −23 °C. In both cities precipitation is quite evenly distributed throughout the year.

During the three years of measurements, the daily snow depths in Helsinki are all below 0.8 m, with a longer snow period in winter 2010/2011 than 2011/2012. The timing of snowpack formation depends strongly on the year. In 2010, it was initiated in November, whereas in the following winter this was delayed until January 2012. This will have a large influence not only on both natural energy and water exchanges, but also urban activities. In Montreal, snowpack depth and timing has large variability between years; for example a 1 m snow pack is observed in March 2008 with melting in late April, compared to only 0.6 m the next year, which was melted by the end of March.

3.2 Model optimization and sensitivity

3.2.1 LAI

Leaf area index (LAI) can be modelled as a function of thermal conditions through growing degree days and senescence degree days, with the thermal threshold being changed to be appropriate for a location (e.g. latitude, continental vs. maritime climate). When LAI is determined using Eq. (4) in Järvi et al. (2011) with coefficient values of $b_1 = b_2 = 0.03$ and $c_1 = c_2 = 5 \times 10^{-4}$, the leaf growth is appropriate in both Helsinki and Montreal. However, the senescence is incorrect with leaves remaining too long (into early December) at both sites despite appropriate thermal conditions being used. To obtain more realistic leaf-off timing parameters, b_2 and c_2 need to be larger. Increasing b_2 to 0.5 and c_2 to 1×10^{-3} makes the leaf-off period more rapid with complete leaf-off by mid-November. This is reasonable for Montreal but still too late for Helsinki. However, when the new senescence parameterization (Eq. 15) based on the day length with parameters $b_3 = -1.5$ and $c_3 = 1.5 \times 10^{-3}$ is used in Helsinki, the timing for leaf fall is more realistic, with leaves gone by the end of October.

3.2.2 Snow properties

The time constants to describe the aging of snow, the minimum and maximum snow albedo, and density were determined by optimization using observations undertaken at the suburban site in Montreal (Pr). The observed snow properties are treated as averages from the measured surface types, in order for them to be compatible with the scale of the simulations. To evaluate the snow albedo, the observed reflected shortwave radiation ($K\uparrow$) in Helsinki in 2011 is used. To assess the radiative exchanges, SUEWS is run using the radiation measurements source area (99 % FOV) estimated as a 31 m radius circle around the 31 m tall measurement tower (Nordbo et al., 2012a). The surface cover characteristics are different for this area to those within the turbulent flux source area; with 49 % paved surface, 4 % buildings, 3 % deciduous trees/shrubs and 44 % grass.

Comparison of our observations with the Lemonsu et al. (2010) (hereafter Le10) aging functions used for the suburban site in Montreal, shows that modifications to the coefficients are needed for both snow albedo and density (Fig. 4). The Le10 maximum density of 350 kg m^{-3} is too small for the current observations. Now, the maximum snow density is set to 400 kg m^{-3}; the minimum value ρ_s^{min} is kept at 100 kg m^{-3}. In addition, the time constant τ_r is decreased to 0.043. After these modifications, the simulated snow density follows the behaviour of the median observations well (Fig. 4a). Similarly from the observations, the minimum (α_s^{min}) and maximum (α_s^{max}) snow albedo are set to 0.18 and 0.85 respectively, which differ from Le10 (α_n^{min} = 0.15–0.30 across the different surface cover types). Le10's snow albedo aging time constants ($\tau_f = 0.174$, $\tau_a = 0.008$) could not be fully evaluated due to lack of data. However, τ_a compared to our observations is too small. This is increased to 0.018, which results in a decrease of τ_f to 0.11. Again good correspondence between the observed snow albedo and model output are seen (Fig. 4b) and between the observed and modelled $K\uparrow$ in Helsinki in 2012 (not shown). During the cold snow period, the linear fit statistics are $S = 0.99 \pm 0.02$ W^{-1} m^2,$I = 0.45 \pm 0.48$ W m^{-2} (RMSE = 11.6 W m^{-2}, $N = 2232$)

GMDD
7, 1063–1114, 2014

Development of the SUEWS for cold climate cities

L. Järvi et al.

and during the warm snow period $S = 0.65 \pm 0.02\,\mathrm{W^{-1}\,m^2}$ and $I = 1.81 \pm 0.56\,\mathrm{W\,m^{-2}}$ (RMSE = $13.9\,\mathrm{W\,m^{-2}}$, $N = 604$). One likely reason for the poorer model performance during the warm snow period is the sensitivity of the albedo to the fraction of snow covered surface. In the model, the fraction of snow is parameterized based on the maximum S_{WE}, but it is likely that this is site dependent at a neighbourhood scale due to redistribution and transport of snow. However, as the other net all-wave radiation components are larger in magnitude than $K\uparrow$, the negative bias during the melting period is likely to have small impact on the available energy.

3.2.3 Melt and freezing factors

The freeze and melt factors (a_{r} and a_{t}), representative for the neighbourhood scale, are optimized using runoff from Pa and snow depth from Ku (Helsinki). SUEWS was run using a_{r} values between 0.0008 and $0.002\,\mathrm{mm\,W^{-1}\,h^{-1}}$ using $0.0001\,\mathrm{mm\,W^{-1}\,h^{-1}}$ resolution, and a_{t} between 0.05 and $0.15\,\mathrm{mm\,^{\circ}C^{-1}\,h^{-1}}$ with $0.01\,\mathrm{mm\,^{\circ}C^{-1}\,h^{-1}}$ resolution. The 146 modelled combinations were analysed with respect to the amount of accumulated melt water during the snow covered period and the timing for complete snow melt (not shown). The smallest differences compared to the observations are obtained with $a_{\mathrm{r}} = 0.0016\,\mathrm{mm\,W^{-1}\,h^{-1}}$ and $a_{\mathrm{t}} = 0.11\,\mathrm{mm\,^{\circ}C^{-1}\,h^{-1}}$. Thus, these are used in the model runs. These are slightly larger, but of the same order of magnitude, to those obtained for hourly factors at an Arctic watershed in Alaska ($a_{\mathrm{r}} = 0.001\,\mathrm{mm\,W^{-1}\,h^{-1}}$ and $a_{\mathrm{t}} = 0.095\,\mathrm{mm\,^{\circ}C^{-1}\,h^{-1}}$; Kane et al., 1997). Unfortunately, no hourly values for urban areas were found in the literature. However, using these factors, the daily melt rates are same order of magnitude than have typically been reported for urban areas (Bengtsson and Semádeni-Davies, 2011).

3.2.4 Snow storage heat

To determine the storage heat flux coefficients a_1, a_2 and a_3 for snow (Eq. 5) shallow water values were used as an initial basis with $a_1 = 0.50$, $a_2 = 0.21$ and $a_3 = -39.1$

GMDD
7, 1063–1114, 2014

(Souch et al., 1998). Given the assumption that the snow heat capacity is around half that of water (Rogers and Yau, 1996), a_1 is set to 0.25 for snow. The other two coefficients (a_2 and a_3) are assessed relative to their effect on the sensible heat flux by running SUEWS for Pr over a range of values. The RMSE between the observed and modelled Q_H varies between 47.8–52.7 W m^{-2} and MBE between −24.9–25.6 W m^{-2}, when a_2 varies between 0 and 0.6 and a_3 between −60 and 0. The optimal result with RMSE = 48.2 W m^{-2} and MBE = 0.19 W m^{-2} is obtained with a_2 = 0.60 and a_3 = −30. Thus, these coefficients are used in the model to calculate the snow storage heat or the internal energy of the snow. The values imply a smaller slope or fraction of radiative energy entering/leaving (a_1), a greater hysteresis (a_2) and a similar phase or time lag (a_3) for snow relative to water. Heuristically this appears appropriate.

3.3 Surface runoff

Figure 5 shows the daily observed and modelled runoff from the two catchments in Helsinki. The grey line separates the non-snow and snow related runoff as the continuous winter snow cover formed on 18 November 2010. At both sites, the model simulates the snow melt induced runoff well, reproducing both the spring melt peak and the recession in April. When the model is run treating the catchments as a whole, it tends to overestimate the runoff peaks and be flashier than observations (Fig. 5), which have smaller but longer runoff peaks. Partly this can be explained by the absence of time lags for the water to move from the most distant points (hydrologically and hydraulically) because the catchment is modelled as one unit (in the current setup). However, in terms of hourly performance, the correlation between the observed (R_{obs}) and modelled (R_{mod}) runoff is good with S = 1.21 (mm h^{-1})$^{-1}$ and I = −0.02 mm h^{-1} (RMSE = 0.15 mm h^{-1}, r = 0.74) in Pa, and S = 1.23 (mm h^{-1})$^{-1}$ (RMSE = 0.16 mm h^{-1}, r = 0.61) in Pi. The coefficients are calculated for periods when both R_{mod} and R_{obs} are non-zero (675 and 760 h in Pa and Pi, respectively). In Pa, the model underestimates the cumulative runoff over the snow covered periods by 10 % as R_{mod} = 77 mm and R_{obs} = 85 mm (Fig. 6).

GMDD
7, 1063–1114, 2014

Despite the slightly poorer correlation in Pi, the cumulative runoff differs only by 6 % as R_{mod} = 86 mm and R_{obs} = 81 mm.

Before the continuous snow cover, the model performs slightly poorer at both catchments. Notably, the model overestimates runoff at Pi with high intensity precipitation. The overestimation is seen in the linear correlation between R_{obs} and R_{mod} as $S = 1.39\,(\text{mm h}^{-1})^{-1}$ and $I = 0.04\,\text{mm h}^{-1}$ (RMSE = 0.21 mm h^{-1}, $r = 0.69$, $N = 668$) as well as in the modelled cumulative runoff, which is 47 % higher than the observed in Pi (27 and 46 mm, respectively) (not shown). In Pa, the model is able to capture the runoff peak better with $S = 1.36\,(\text{mm h}^{-1})^{-1}$ and $I = -0.01\,\text{mm h}^{-1}$ (RMSE = 0.23 mm h^{-1}, $r = 0.89$, $N = 743$), and the cumulative runoff is 11 % underestimated by the model (R_{obs} = 84 mm and R_{mod} = 93 mm). Some of these differences are caused by the forcing precipitation and other meteorological variables being from the flux site Ku. This would particularly affect the model performance during convective precipitation, which accounts for 88 % of the precipitation events between April and September (Punkka and Bister, 2005).

3.4 Snow depth

The model calculates snow water equivalent (S_{WE}) and snow depth (s_d) separately for each surface type. Due to snow removal and the different surface characteristics, s_d behaves differently for the vegetated and built surfaces. This can be seen when the modelled s_d for each surface (paved, building, grass and tree) is plotted with the observations for Helsinki (Fig. 7) and Montreal (Fig. 8). Unfortunately, the observations are each representative of individual point and surface types, whereas the model values are for the different surface types at the neighbourhood scale. Thus, some differences between the modelled and observed s_d are expected.

In Helsinki, the point observations are made in an open space that corresponds most appropriately to the modelled grass surface. Data for 2011 and 2012 are plotted separately as the first year is used in the model parameter determination whereas the latter is an independent dataset (Fig. 7). In both years, the model reproduces the accumulation of snow and melt events well, but underestimates the snow depth by around 100 mm compared to the observations. The measured maximum snow depth in 2011 is 720 mm, whereas the modelled snow depth above grass is 587 mm. Similarly, for 2012 the observed depth is 630 mm and the modelled value is 505 mm. This underestimation is caused by either the underestimation of modelled S_{WE} or by overestimation of snow density as the snow depth is a function of these two variables (Eq. 14). The model starts to accumulate snow four days later than the observations in January 2012, but later in the year the observed and modelled snow cover appear on the exact date 29 November. In 2011, the snow melt is observed to be completed on 15 April, five days earlier than simulated, whereas in 2012 the snow melt is finished on 12 April, one day later than modelled.

For Montreal, s_d is calculated separately for the suburban (Pr) and urban (RI) sites for January 2008–April 2009. In Pr, the observations are made on lawn corresponding to the modelled grass surface (Fig. 8a). The model follows the accumulation and melt events well, but like Helsinki, snow depths are underestimated especially in the 2007–2008 winter. The maximum observed s_d is 1020 mm, while 680 mm was modelled for grass. In winter 2008–2009, the maximum observed and simulated snow depths are 660 and 467 mm. In 2008, the modelled snow starts to accumulate on the same day (8 December) as observed. Snow melt is completed on 20 April 2008, which is three days after the modelled date. In 2009 the modelled snow melt finishes one day before observed (30 March).

In RI, s_d is observed on a building roof which results in both lower snow amounts and earlier melt compared to the lawn observations in Montreal (Fig. 8b). The model simulates this behaviour well, but again under predicts the depths. The observed s_d maxima are 390 and 415 mm for the two winters, while 285 and 276 mm are modelled, respectively. Accumulation of snow takes place on the correct day in RI, and the snow melts on the same day as observed on 26 March 2008, and nine days later on 7 March 2009 than observed.

GMDD
7, 1063–1114, 2014

3.5 Turbulent and radiative energy fluxes

The simulated Q^*, Q_H and Q_E are assessed for snow-free, cold snow and warm snow periods (Table 4, Fig. 9), with the diurnal behaviour of both the observed and modelled fluxes for the independent datasets in Helsinki and Montreal considered (Figs. 10 and 11).

Generally the best simulated flux of the three is Q^* independent of whether there is snow on the ground or not. For the cold and warm snow periods, the RMSE varies between 26–48 W m^{-2} (nRMSE = 0.0036–0.071) and 30–42 W m^{-2} (nRMSE = 0.04–0.058) across the sites. At all sites, Q^* is underestimated in cold snow conditions with MBE between −36 and −13 W m^{-2}. Mostly this underestimation is related to the downward long-wave radiation that is calculated from air temperature and relative humidity (Loridan et al., 2011 – who suggest that this technique does not work as well when using cloud cover data are used as input). This parameterization works less well in cold conditions than above 0 °C. In Montreal, the warm snow underestimation is even larger (MBE = −35 to −24 W m^{-2}), compared to Helsinki where the underestimation decreases to −3 to −2 W m^{-2}. Especially during the warm snow periods, the fraction of snow cover plays an important part in the model performance. It affects both the snow albedo and outgoing long-wave radiation via surface temperature. The best performance for Q^* is under snow free conditions, when the MBE is between −10 and 8 W m^{-2} and the nRMSE is clearly lower than for the periods with snow cover (Fig. 9a).

The scatter in the model performance is larger for Q_E than for the other energy balance components, with cold snow periods having the best and warm snow periods the poorest model performance (Fig. 9c). The RMSE during cold snow varies between 9–12 W m^{-2} (nRMSE = 0.036–0.058), and for warm snow between 22–40 W m^{-2} (nRMSE = 0.067–0.200). The increase in RMSE during warm snow periods is understandable as the energy consumed in melting snow and freezing melt water is higher and thus errors in the degree-day-method propagate more easily to Q_E (as well as to Q_H). During melting periods there can be advection from snow-free surfaces to the snowpack altering the energy balance as specified in Eq. (1) (Bengtsson and Semádeni-Davies, 2011). MBE varies between -11–$5.4\,\mathrm{W\,m^{-2}}$ when there is snow on ground. During snow free periods, the model underestimates Q_E at all sites with MBEs between -28 to $-12\,\mathrm{W\,m^{-2}}$, RMSEs between 24–33 $\mathrm{W\,m^{-2}}$, and nRMSE between 0.055–0.064.

In SUEWS, Q_H is calculated as a residual from other energy fluxes; therefore the net error accumulates in Q_H. Despite this, the model is able to simulate its behaviour well. When there is snow on ground, the RMSE varies between 22–50 $\mathrm{W\,m^{-2}}$ and nRMSE between 0.065 and 0.118. During the cold snow periods, the simulated heat fluxes are slightly better than during warm snow periods, similar to Q_E. The model overestimates Q_H during snow cover, except in RI during cold snow periods, and MBEs vary between -17–$12\,\mathrm{W\,m^{-2}}$. In summer, the performance of the model in simulating Q_H improves following the performance of Q^* and Q_E.

The model performance for the energy fluxes is more dependent on the period of analysis than the site where it is run. An exception to this is Q_H at RI, where the model overestimates and shifts the diurnal peak flux earlier compared to the observations (Fig. 11). This appears whether there is snow on ground or not, suggesting that this is caused by the snow free storage heat flux which is underestimated or anthropogenic heat flux that is overestimated by the model. RMSEs obtained for the warm snow periods in Pr are higher than Le10 obtained for the same suburban area in Montreal using the Town Energy Balance model in spring 2005. However, direct comparisons are difficult as in their one month of observations snow cover is present only on some days compared to the longer time period evaluated here.

3.6 Energy balance of urban snow covered surface

Snow cover and the related energy storage and the energy related to phase change alter the surface energy balance. The components at the most built-up site RI are evaluated here (Fig. 12). During cold snow periods, the daytime energy balance is

GMDD
7, 1063–1114, 2014

dominated by the net all-wave radiation (Q^*) and the sensible heat flux (Q_H), both reaching $96\,W\,m^{-2}$. Q_H is fuelled by both Q^* and Q_F (reaching $40\,W\,m^{-2}$), and it accounts on average for 74 % of the daytime (10:00–15:00) available energy. The dominance of Q^* and Q_H are typical also for natural cold snow packs (e.g. Oke, 1987). Only 15 % of $Q^* + Q_F$, is dissipated by evaporation, whereas the storage fractions are 9 and 3 % at the snow and snow free surfaces, respectively. At night, on the other hand, the urban surface loses long-wave radiation causing the internal energy of the snow to decrease i.e. the cold content of the snow increases. At the same time, the snow free surface loses some energy (around 9–10 $W\,m^{-2}$) and both Q_F and Q_E remain positive (by more than $10\,W\,m^{-2}$), with Q_H less than $5\,W\,m^{-2}$.

During warm snow periods, Q^* is clearly the most important component of the surface energy balance reaching $200\,W\,m^{-2}$ in daytime. Now the daytime Q_F is slightly smaller than during the cold periods reaching $35\,W\,m^{-2}$. Most of the energy, but clearly less than during the cold snow period, is partitioned to Q_H (45 %), with the second largest contribution going to snow free surface heat storage (30 %). Evaporation consumes 17 % of the energy and only 4 % is stored in the snow and consumed by snow melt. The largest Q_H and ΔQ_S are consistent with the observations obtained by Le10 at the suburban site, although they documented a larger contribution going to snow related processes than to evaporation. Moreover, the modelled fractions during the snow covered periods are of the same order of magnitude as obtained for observations at the same site (Bergeron and Strachan, 2012).

When the ground is free of snow, most energy ($Q^* + Q_F$) again goes to Q_H ($190\,W\,m^{-2}$, 46 %) followed by the storage heat flux ($175\,W\,m^{-2}$, 42 %). Due to the high impervious nature of the surface, daytime Q_E reaches $48\,W\,m^{-2}$, which is only 12 % of the available energy. The resulting daytime Bowen ration (Q_H/Q_E) is 3.9, which corresponds well with the expected relationship of the Bowen ratio with the sites vegetation fraction (Loridan and Grimmond, 2012).

4 Conclusions

The Surface Urban Energy and Water balance Scheme (SUEWS) is developed to simulate the energy and water balances in cold climate cities with special attention on the simulation of snow cover. The new model considers the accumulation of snow, snow properties including snow water equivalent, snow depth, snow density and albedo, and snow melt and refreezing of melt water based on an hourly degree-day method. The development and independent evaluation is undertaken using observations from three sites in Helsinki and two sites in Montreal. Each of these sites varies in terms of surface cover characteristics. In Helsinki, the observations include stormwater runoff from two catchments and turbulent fluxes of sensible and latent heat from one site. In Montreal, the observations include snow properties as well as the turbulent fluxes at both sites.

The model developments include an improved description of vegetation phenology (LAI) in cold climate cities. The leaf-off period based on daily air temperature was accelerated, using a combination of daily air temperatures and day length. Updated aging functions for snow density and albedo in urban areas were developed based on snow observations in Montreal an improved equation for the degree day method was used to calculate snow melt and freezing of the melted water, and new parameter values developed to calculate the snow storage heat flux using the objective hysteresis model (OHM).

The enhanced model can correctly simulate the winter and springtime melt-related runoff, but the runoff peaks tend to be sharper than the observations partly due to the absence of time lag to let the water flow to the observation point at the catchment discharge point. Despite this, the modelled cumulative runoff during the snow covered periods corresponds well with the observations. The formation and melting of the snowpack is simulated well both in Helsinki and Montreal, but the snow depth is underestimated either due to overestimation of the snow density or underestimation of snow water equivalent. Following the hydrological variables, the net radiation and turbulent sensible and latent heat fluxes also are modelled well. The model simulates

GMDD
7, 1063–1114, 2014

their diurnal behaviour throughout the year, but the largest uncertainties occur during the snow melt period at all sites. This is related to the uncertainties in determining the snow covered surface fractions, as well as the propagating uncertainties from the calculation of melt and freezing related energies based on the degree-day method.

The model can correctly simulate the energy and water cycles in cold climate cities and it can be used independently in urban planning purposes or nested to a meso- or global scale atmospheric model. However, some of the parameterizations are still city and site dependent; more observations from cold climate cities are needed to create more generalized formulations.

Acknowledgements. This work was supported by the Academy of Finland (Project numbers 138328 and ICOS-Finland, 263149), and the EU-funded-project BRIDGE. The Montreal data were obtained as part of the Environmental Prediction in Canadian Cities Research network and funded through a grant from the Natural Sciences and Engineering Research Council of Canada. We thank: Erkki Siivola and Petri Keronen for the instrument maintenance of the eddy covariance setups in Helsinki; Eric Christensen for the collection of snow data in Montreal; and Onil Bergeron for the eddy covariance data quality in Montreal. A compiled version of the model with manual and example input and output files can be obtained from http://LondonClimate.info. If you are interested in the code itself please contact Sue Grimmond (C.S.Grimmond@reading.ac.uk)

References

Anderson, E. A.: A point energy and mass balance model of a snow cover, NOAA Technical Report NWS 19, 61–62, 1976.

Auer, A. H.: The rain versus snow threshold temperatures, Weatherwise, 27, p. 67, doi:10.1080/00431672.1974.9931684, 1974.

Baker, D. G., Ruschy, D. L., and Wall, D. B.: The albedo decay of prairie snows, J. Appl. Meteorol., 29, 179–187, 1990.

Bengtsson, L.: The importance of refreezing on the diurnal snowmelt cycle with application to a Northern Swedish catchment, Nord. Hydrol., 13, 1–12, 1982.

Bengtsson, L.: Modeling snowmelt induced runoff with short time resolution, Proceedings of 3rd International Conference of Urban Storm Drainage, Gothenburg, Sweden, 305–314, 1984.
Bengtsson, L. and Semádeni-Davies, A. F.: Urban snow, in: Encyclopedia of Snow, Ice and Glaciers, edited by: Singh, V. P., Singh, P., and Haritashya, U. K., Springer Science, 1211–1217, 2011.
Bengtsson, L. and Westerström, G.: Urban snowmelt and runoff in northern Sweden, Hydrolog. Sci. J., 37, 263–275, 1992.
Bergeron, O. and Strachan, I. B.: Wintertime radiation and energy budget along an urbanization gradient in Montreal, Canada, Int. J. Climatol., 32, 137–152, 2012.
Best, M. J. and Grimmond, C. S. B.: Analysis of the seasonal cycle within the first international urban land-surface model comparison, Bound.-Lay. Meteorol., 146, 421–446, 2013.
Cline, D. W.: Snow surface energy exchanges and snowmelt at a continental, midlatitude Alpine site, Water Resour. Res., 33, 689–701, 1997.
Daley, R.: Atmospheric Data Analysis, Cambridge University Press, Cambridge, UK, 1991.
Debele, B., Srinivasan, R., and Gosain, A. K.: Comparison of process-based and temperature-index snowmelt modeling in SWAT, Water Resour. Manag., 24, 1065–1088, 2010.
Easton, Z. M., Gérard-Marchant, P., Walter, M. T., Petrovic, A. M., and Steenhuis, T. S.: Hydrologic assessment of an urban variable source watershed in the northeast United States, Water Resour. Res., 43, W03413, doi:10.1029/2006WR005076, 2007.
Ek, M. B., Mitchell, K. E., Lin, Y., Rogers, E., Grunmann, P., Koren, V., Gayno, G., and Tarpley, J. D.: Implementation of Noah land surface model advances in the National Centers for Environmental Prediction operational mesoscale Eta model, J. Geophys. Res., 108, 8851, doi:10.1029/2002JD003296, 2003.
Grimmond, C. S. B., Cleugh, H. A., and Oke, T. R.: An objective urban heat storage model and its comparison with other schemes, Atmos. Environ. B-Urb., 25, 311–174, 1991.
Grimmond, C. S. B., Blackett, M., Best, M. J., Baik, J.-J., Belcher, S. E., Beringer, J., Bohnenstengel, S. I., Calmet, I., Chen, F., Coutts, A., Dandou, A., Fortuniak, K., Gouvea, M. L., Hamdi, R., Hendry, M., Kanda, M., Kawai, T., Kawamoto, Y., Kondo, H., Krayenhoff, E. S., Lee, S.-H., Loridan, T., Martilli, A., Masson, V., Miao, S., Oleson, K., Ooka, R., Pigeon, R., Porson, A., Ryu, Y.-H., Salamanca, F., Steeneveld, G. J., Tombrou, M., Voogt, J. A., Young, D. T., and Zhang, N.: Initial results from phase 2 of the international urban energy balance model comparison, Int. J. Climatol., 31, 244–272, doi:10.1002/joc.2227, 2011.

Jacobson, C. R.: Identification and quantification of the hydrological impacts of imperviousness in urban catchments: a review, J. Environ. Manage., 92, 1438–1448, 2011.
Järvi, L., Hannuniemi, H., Hussein, T., Junninen, H., Aalto, P. P., Hillamo, R., Mäkelä, T., Keronen, P., Siivola, E., Vesala, T., and Kulmala, M.: The urban measurement station SMEAR III: continuous monitoring of air pollution and surface-atmosphere interactions in Helsinki, Finland, Boreal Environ. Res., 14, 86–109, 2009a.
Järvi, L., Mammarella, I., Eugster, W., Ibrom, A., Siivola, E., Dellwik, E., Keronen, P., Burba, G., and Vesala, T.: Comparison of net CO_2 fluxes measured with open- and closed-path infrared gas analyzers in urban complex environment, Boreal Environ. Res., 14, 499–514, 2009b.
Järvi, L., Grimmond, C. S. B., and Christen, A.: The surface urban energy and water balance scheme (SUEWS): evaluation in Los Angeles and Vancouver, J. Hydrol., 411, 219–237, 2011.
Järvi, L., Nordbo, A., Junninen, H., Riikonen, A., Moilanen, J., Nikinmaa, E., and Vesala, T.: Seasonal and annual variation of carbon dioxide surface fluxes in Helsinki, Finland, in 2006–2010, Atmos. Chem. Phys., 12, 8475–8489, doi:10.5194/acp-12-8475-2012, 2012.
Jin, J., Gao, X., Sorooshian, S., Yang, Z.-L., Bales, R., Dickinson, R. E., Sun, S.-F., and Wu, G.-X.: One-dimensional snow water and energy balance model for vegetated surfaces, Hydrol. Process., 13, 2467–2482, 1999.
Kane, D. L, Gieck, R. E., and Hinzman, L. D.: Snowmelt modeling at small Alaskan Arctic watershed, J. Hydrol. Eng., 2, 204–210, 1997.
Keskitalo, J., Bergquist, G., Gardeström, P., and Jansson, S.: A cellular timetable of autumn senescence, Plant Physiol., 139, 1635–1648, 1995.
Koivusalo, H. and Kokkonen, T.: Snow processes in a forest clearing and in a coniferous forest, J. Hydrol., 262, 145–164, 2002.
Kustas, W. P., Rango, A., and Uijlenhoet, R.: Simple energy budget algorithm for the snowmelt runoff model, Water Resour. Res., 30, 1515–1527, 1994.
Lemonsu, A., Bélair, S., Mailhot, J., Benjamin, M., Chagnon, F., Morneau, G., Harvey, B., Voogt, J., and Jean, M.: Overview and first results of the Montreal urban snow experiment 2005, J. Appl. Meteorol. Clim., 47, 59–75, 2008.
Lemonsu, A., Bélair, S., Mailhot, J., and Leroyer, S.: Evaluation of the town energy balance model in cold and snowy conditions during the Montreal urban snow experiment 2005, J. Appl. Meteorol. Clim., 49, 346–362, 2010.

Leroyer, S., Mailhot, J., Bélair, S., Lemonsu, A., and Strachan, I. B.: Modeling the surface energy budget during the thawing period of the 2006 Montreal urban snow experiment, J. Appl. Meteorol. Clim., 49, 68–84, 2010.
Loridan, T. and Grimmond, C. S. B.: Characterization of energy flux partitioning in urban environments: Links with surface seasonal properties, J. Appl. Meteorol. Clim., 51, 219–241, 2012.
Loridan, T., Grimmond, C. S. B., Offerle, B. D., Young, D. T., Smith, T., Järvi, L., and Lindberg, F.: Local-scale Urban Meteorological Parameterization Scheme (LUMPS): longwave radiation parameterization and seasonality related developments, J. Appl. Meteorol. Clim., 50, 185–202, doi:10.1175/2010JAMC2474.1, 2011.
Lowe, P. R.: An approximation polynomial for the computation of saturation vapor pressure, J. Appl. Meteorol., 16, 100–103, 1977.
Martine, G. and Marshall, A.: State of World Population 2007: Unleashing the Potential of Urban Growth, U. N. Popul. Fund, New York, 2007.
Martinec, J.: Hour-to-hour snowmelt rates and lysimeter outflow during an entire ablation period, Snow cover and Glacier Variations, Proceedings of the Baltimore Symposium, Maryland, IAHS Publ. 183, 1989.
Mitchell, V. G., McMahon, T. A., and Mein, R. G.: Components of the total water balance of an urban catchment, Environ. Manage., 32, 735–746, 2003.
Mitchell, V. G., Cleugh, H. A., Grimmond, C. S. B., and Xu, J.: Linking urban water balance and energy balance models to analyze urban design options, Hydrol. Process., 22, 2891–2900, 2008.
Nordbo, A., Järvi, L., and Vesala, T.: Revised eddy covariance flux calculation methodologies – effect on urban energy balance, Tellus B, 48, 18184, doi:10.3402/tellusb.v64i0.18184, 2012a.
Nordbo, A., Järvi, L., Haapanala, S., Moilanen, J., and Vesala, T.: Intra-city variation in urban morphology and turbulence structure in Helsinki, Finland, Bound.-Lay. Meteorol., 146, 469–496, doi:10.1007/s10546-012-9773-y, 2012b.
Offerle, B., Grimmond, C. S. B., and Oke, T. R.: Parameterization of net all-wave radiation for urban areas, J. Appl. Meteorol., 42, 1157–1173, 2003.
Oke, T.: Boundary Layer Climates, Routledge, London, UK, 1987.

GMDD
7, 1063–1114, 2014

Development of the SUEWS for cold climate cities

L. Järvi et al.

Punkka, A. J. and Bister, M.: Occurrence of summertime convective precipitation and mesoscale convective systems in Finland during 2000–01, Mon. Weather Rev., 133, 362–373, 2005.
Rogers, R. R. and Yau, M. K.: A Short Course in Cloud Physics, Elsevier Science, Oxford, UK, 1996.
Semádeni-Davies, A. F.: Snow heterogeneity in Luleå, Sweden, Urban Water J., 1, 39–47, 1999.
Semádeni-Davies, A. F. and Bengtsson, L.: Snowmelt sensitivity to radiation in the urban environment, Hydrolog. Sci. J., 43, 67–89, 1998.
Semádeni-Davies, A. F. and Bengtsson, L.: The water balance of sub-arctic town, Hydrol. Process., 13, 1871–1885, 1999.
Semádeni-Davies, A., Lundberg, A., and Bengtsson, L.: Radiation balance of urban snow: a water management perspective, Cold Reg. Sci. Technol., 33, 59–76, 2001.
Souch, C., Grimmond, C. S. B., and Wolfe, C. P.: Evaporation rates from wetlands with different disturbance histories: Indiana dunes national lakeshore, Wetlands, 18, 216–229, 1998.
Sun, S., Jin, J., and Xue, Y.: A simple snow-atmosphere-soil transfer model, J. Geophys. Res., 104, 19587–19597, 1999.
Swenson, S. C. and Lawrence, D. M.: A new fractional snow-covered area parameterization for the community land model and its effect on the surface energy balance, J. Geophys. Res., 117, D21107, doi:10.1029/2012JD018178, 2012.
Tobin, C., Schaefli, B., Nicótina, L., Simoni, S., Barrenetxea, G., Smith, R., Parlange, M., and Rinaldo, A.: Improving the degree-day method for sub-daily melt simulations with physically-based diurnal variations, Adv. Water Resour., 55, 149–164, 2013.
Valeo, C. and Ho, C. L. I.: Modelling urban snowmelt runoff, J. Hydrol., 299, 237–251, 2004.
Valtanen, M., Sillanpää, N., and Setälä, H.: Effects of land use intensity on stormwater runoff and its temporal occurence in cold climates, Hydrol. Process., 28, 2639–2650, doi:10.1002/hyp.9819, 2013.
Vargo, J., Habeeb, D., and Stone Jr., B.: The importance of land cover change across urban-rural typologies for climate modelling, J. Environ. Manage., 114, 243–252, 2013.
Verseghy, D. L.: CLASS – A Canadian Land Surface Scheme for GCMS, 1, soil model, Int. J. Climatol., 11, 111–133, 1991.

GMDD
7, 1063–1114, 2014

Development of the SUEWS for cold climate cities

L. Järvi et al.

Vesala, T., Järvi, L., Launiainen, S., Sogachev, A., Rannik, Ü., Mammarella, I., Siivola, E., Keronen, P., Rinne, J., Riikonen, A., and Nikinmaa, E.: Surface-atmosphere interactions over complex urban terrain in Helsinki, Finland, Tellus B, 60, 188–199, 2008.

Voogt, J. A. and Grimmond, C. S. B.: Modeling surface sensible heat flux using surface radiative temperatures in a simple urban area, J. Appl. Meteorol., 39, 1679–1699, 2000.

GMDD

7, 1063–1114, 2014

Table 1. Site characteristics of the observational sites. Surface cover fractions for the EC sites are calculated for 1 km radius circles, whereas the fractions of the catchments are for the actual catchment areas. In Kumpula, the area is divided into three surface cover areas (Ku1, Ku2 and Ku3). For the abbreviations, see Appendix A.

	Helsinki Kumpula			Pasila	Pihlajamäki	Montreal Urban	Suburban
Lat	60.203° N			60.199° N	60.238° N	45.457° N	45.501° N
Lon	24.961° E			24.940° E	25.014° E	73.592° W	73.811° W
Obs.	Q^*, Q_H, Q_E, met			R	R	Q^*, Q_H, Q_E, met.	Q^*, Q_H, Q_E, met.
z (m)	31			–	–	25	25
Site name	Ku1	Ku2	Ku3	Pa	Pi	Rl	Pr
λ_{pav}	0.42	0.39	0.30	0.42	0.22	0.44	0.37
λ_{bldg}	0.20	0.15	0.11	0.20	0.12	0.27	0.12
λ_{veg}	0.38	0.46	0.59	0.38	0.66	0.29	0.50
λ_{everg}	0.01	0	0.01	0	0.10	0	0.05
λ_{dec}	0.21	0.20	0.30	0.24	0.30	0.03	0.15
λ_{igrass}	0.15	0.20	0.21	0.10	0.02	0.20	0.25
λ_{grass}	0.01	0.06	0.10	0.02	0.1	0.06	0.05
λ_{unman}	0	0	0	0.02	0.14	0	0
λ_{water}	0	0.01	0.00	0	0	0	0.01
z_h(m)	10.4	11.5	12.6	15.2	10.8	7.9	6.4
z_t(m)	10	8.8	8.5	8	8	13.0	13.8
p (# ha^{-1})	31	37	44	42	55	84	24
A (ha)	44.7	78.2	78.2	23.8	44.8	314.2	314.2
Reference	Järvi et al. (2009a)			–	–	Bergeron and Strachan (2012)	

GMDD
7, 1063–1114, 2014

Development of the SUEWS for cold climate cities

L. Järvi et al.

Title Page
Abstract Introduction
Conclusions References
Tables Figures
◀◀ ▶▶
◀ ▶
Back Close
Full Screen / Esc
Printer-friendly Version
Interactive Discussion

Table 2. Time period and the spin-up time of the model simulations. Data availability is the number of 60 min periods when observations are available for the non-spin-up period. EC is the eddy covariance fluxes (Q_H and Q_E), R is the runoff and s_d the snow depth. A sub-set of these data are used in parameter optimization and another for evaluation.

		Measurement period	Spin-up period	Data availability during non-spin-up (%)
Ku	EC	2010–2012	Jan–Aug 2010	44
	s_d			100
Pa	R	Sep 2010–Apr 2011	Jan–Aug 2010	93
Pi	R			86
Pr	EC	Dec 2007–Sep 2009	Dec 2007	53
	s_d			80
Rl	EC	Dec 2007–Sep 2009	Dec 2007	36
	s_d			85

GMDD
7, 1063–1114, 2014

Table 3. Parameters used in SUEWS for surfaces that are buildings (bldg), pavement (pav), evergreen vegetation (everg), deciduous vegetation (decid), grass and water. If the vegetation is irrigated, different values to describe the canopy are used. Sources of the values are as in Järvi et al. (2011) unless indicated otherwise below. Where different values are used for the different sites, this is indicated for Helsinki (Hel) and for the two sites in Montreal (Rl and Pr). Variable notation is given in Appendix A .

a)	Site	Units	Bldg	Pav	Everg.	Decid.	Irr. veg	Grass	Water
S_i		mm	0.25	0.48	1.3	0.3–0.8		1.9	0
$S_{\mathrm{soil},i}$	Hel/Rl	mm	50	100	150	150	150	150	–
	Pr	mm	150	150	150	150	150	150	–
$D_{0,i}$		mm	10	10	0.013	0.013	10	0.013	–
b		–	3	3	1.71	1.71	0.013	1.71	–
C_i		mm	0	0	0	0	0	0	0
$C_{\mathrm{soil},i}$	Hel/Rl	mm	50	100	150	150	150	150	–
	Pr	mm	150	150	150	150	150	150	–
α_i		–	0.15	0.09[a]	0.10	0.16[b]	0.19	0.19[b]	0.08[b]
ε_i		–	0.95	0.91	0.98	0.98	0.93	0.93	0.95
$g_{i,\max}$		$\mathrm{mm\,s^{-1}}$	–	–	7.4	11.7	40	33.1	–
Snow									
$S_{\mathrm{WE},0}$	Hel	mm	40	40	40	40	40	40	40
	Mon	mm	0	0	0	0	0	0	0
$f_{\mathrm{s},i,0}$	Hel	mm	1	1	1	1	1	1	1
	Mon	mm	0	0	0	0	0	0	0
$\rho_{\mathrm{s},0}$		$\mathrm{kg\,m^{-3}}$	120	120	120	120	120	120	120
$S_{\mathrm{WE},i}^{max}$		mm	190	190	190	190	190	190	–
$S_{\mathrm{WE,Lim}}$		mm	40	100					

b) Overall area parameter values							
$\alpha_s^{\min}$	0.18	$a_{0,\mathrm{wd,we}}$	$0.1\,\mathrm{W\,m^{-2}\,(p^{-1}\,ha^{-1})^{-1}}$[a]	G_4	$3.36\,\mathrm{g\,kg^{-1}}$	$\mathrm{res_{cap}}$	10 mm
$\alpha_s^{\max}$	0.85	$a_{1,\mathrm{wd,we}}$	$9.9\times10^3\,\mathrm{W\,m^{-2}\,K^{-1}\,(p^{-1}\,ha^{-1})^{-1}}$	G_5	11.07 °C	$\mathrm{res_{drain}}$	$0.25\,\mathrm{mm\,h^{-1}}$
ε_s	0.99	$a_{2,\mathrm{wd,we}}$	$0.0102\,\mathrm{W\,m^{-2}\,K^{-1}\,(p^{-1}\,ha^{-1})^{-1}}$	G_6	0.018 mm	R_C	1.0 mm
ρ_e	$200\,\mathrm{kg\,m^{-3}}$	$b_{0,a}$	−84.54 mm	GDD	300	S_1	0.45 mm
$\rho_s^{\min}$	$100\,\mathrm{kg\,m^{-3}}$	$b_{1,a}$	$9.96\,\mathrm{mm\,K^{-1}}$	I_w	0 mm	S_2	15 mm
$\rho_s^{\max}$	$400\,\mathrm{kg\,m^{-3}}$	$b_{2,a}$	$3.67\,\mathrm{mm\,d^{-1}}$	$K\downarrow_\mathrm{m}$	$1200\,\mathrm{W\,m^{-2}}$	S_Pipe	100 mm
τ_a	0.018	$b_{0,m}$	−25.36 mm	K_s	$0.0005\,\mathrm{mm\,s^{-1}}$	SDD	−450
τ_f	0.11	$b_{1,m}$	$3.00\,\mathrm{mm\,K^{-1}}$	$\mathrm{LAI_{max,everg}}$	$5.1\,\mathrm{m^2\,m^{-2}}$	T_BaseGDD	5 °C
a_1	0.25	$b_{2,m}$	$1.10\,\mathrm{mm\,d^{-1}}$	$\mathrm{LAI_{max,dec}}$	$5.5\,\mathrm{m^2\,m^{-2}}$	T_BaseSDD	10 °C
a_2	0.6	$C_{\min}^R$	0.05 mm	$\mathrm{LAI_{max,grass}}$	$5.9\,\mathrm{m^2\,m^{-2}}$	T_BaseQF	18.2 °C
a_3	−30	$C_{\max}^R$	0.2 mm	$\mathrm{LAI_{min,everg}}$	$4.0\,\mathrm{m^2\,m^{-2}}$	T_lim	2.2 °C[c]
a_f	1	G_1	$16.48\,\mathrm{mm\,s^{-1}}$	$\mathrm{LAI_{min,dec}}$	$1.0\,\mathrm{m^2\,m^{-2}}$	T_H	40 °C
a_r	$0.0016\,\mathrm{mm\,W^{-1}\,h^{-1}}$	G_2	$566.1\,\mathrm{W\,m^{-2}}$	$\mathrm{LAI_{min,grass}}$	$1.6\,\mathrm{m^2\,m^{-2}}$	T_L	10 °C
a_t	$0.011\,\mathrm{mm\,^{\circ}C^{-1}\,h^{-1}}$	G_3	$0.216\,\mathrm{kg\,g^{-1}}$	$r_{\mathrm{s,max}}$	$9999\,\mathrm{s\,m^{-1}}$	T_step	300 s

[a] Optimized using data from Helsinki.
[b] Vargo et al. (2013).
[c] Auer (1974)

GMDD
7, 1063–1114, 2014

Development of the SUEWS for cold climate cities

L. Järvi et al.

Table 4. Model evaluation statistics based on performance relative to observations of net all wave radiation (Q^*, W m^{-2}), sensible (Q_H, W m^{-2}) and latent heat fluxes (Q_E, W m^{-2}) undertaken for two years in Helsinki (Ku11 for 2011 and Ku12 for 2012) and two sites in Montreal (Pr and Rl). The statistics: S ((W m^{-2})$^{-1}$) and I (W m^{-2}) are the linear fit regression coefficients $y = Sx + I$, RMSE is the root mean square error (W m^{-2}), nRMSE the normalized RMSE, and N is the number of points in the linear fit.

		Cold snow						Melting snow						Snow-free					
		S	I	RMSE	nRMSE	N	MBE	S	I	RMSE	nRMSE	N	MBE	S	I	RMSE	nRMSE	N	MBE
Ku11	Q^*	0.89	−12.4	33.2	0.043	1697	−12.6	1.06	−7.5	38.8	0.05	1032	−3.1	0.98	8.3	30.3	0.03	5980	7.8
	Q_H	0.72	4.4	26.2	0.065	756	−8.2	0.51	21.4	49.1	0.098	440	−15.8	0.7	22.3	38	0.064	3064	0.6
	Q_E	0.52	8.9	12.2	0.038	613	−1.9	0.81	7.8	22.3	0.067	381	−10	0.54	5.3	24.1	0.055	2623	−25.6
Ku12	Q^*	0.62	−30.6	25.6	0.036	2238	−31.6	1.11	−6.3	41.5	0.058	674	−1.8	1	4.9	29	0.03	5554	7.5
	Q_H	0.53	−7.2	21.8	0.069	1056	−25.2	0.73	14.1	38.1	0.083	299	−12.1	0.64	20.9	38.8	0.056	3414	−6.8
	Q_E	0.18	9.6	10.1	0.045	775	−5.5	0.59	5	24.5	0.109	233	−10.8	0.59	2.8	25.5	0.064	2856	−28.3
Pr	Q^*	0.69	−26.8	39.6	0.057	2980	−36.1	1.01	−21	30.4	0.04	1158	−34.9	0.95	4.8	24.6	0.028	6939	−4.3
	Q_H	0.82	0	33.9	0.086	2177	−8.7	0.98	−2	49.6	0.118	683	−16	0.7	13.8	31.9	0.069	5587	−9.8
	Q_E	0.41	9.8	10.7	0.036	2063	1.7	0.84	16.5	40	0.2	661	5.4	0.73	5.7	33	0.063	5451	−14.7
Rl	Q^*	0.89	−11.8	47.6	0.071	2740	−14.4	1.04	−14.8	31.6	0.042	1014	−23.5	0.99	13	26.6	0.032	4472	−9.5
	Q_H	0.96	15.2	34.4	0.075	1366	8.2	0.82	11.2	43.4	0.09	547	−16.9	0.92	16.6	47.7	0.086	3737	−8.6
	Q_E	0.52	7	8.5	0.058	1292	1.3	0.38	18.2	24.2	0.123	524	4.3	0.47	5.3	26.7	0.061	3636	−11.9

GMDD
7, 1063–1114, 2014

Table A1. Nomenclature.

α_i	Effective surface albedo (–)
α_s	Effective snow albedo (–)
α_s^{min}	Minimum snow albedo (–)
α_s^{max}	Minimum snow albedo (–)
ΔQ^*	Change in the net-all wave radiation in time step Δt (W m^{-2})
ΔQ_A	Advective heat flux (W m^{-2})
$\Delta Q_{S,I}$	Change in the snow heat storage (W m^{-2})
ΔS_{WE}	Change in the snow water equivalent (mm h^{-1})
Δt	Time step of the model (s)
ε_i	Effective surface emissivity (–)
ε_s	Effective surface emissivity of snow (–)
γ	Psychometric constant (Pa °C^{-1})
λ_{bldg}	Surface fraction of buildings (–)
λ_{dec}	Surface fraction of deciduous trees (–)
λ_{ev}	Surface fraction of evergreens (–)
λ_{grass}	Surface fraction of non-irrigated grass (–)
λ_{igrass}	Surface fraction of grass (–)
λ_{pav}	Surface fraction of paved areas (–)
λ_{unman}	Surface fraction of unmanaged land (–)
λ_{veg}	Surface fraction of vegetation (–)
λ_{water}	Surface fraction of water (–)
ρ	Air density (kg m^{-3})
ρ_e	Threshold value in the calculation of retention capacity (kg m^{-3})
ρ_s	Snow density (kg m^{-3})
$\rho_{s,0}$	Initial snow density (kg m^{-3})
ρ_w	Water density (kg m^{-3})
ρ_s^{max}	Maximum snow density (kg m^{-3})
ρ_s^{min}	Minimum snow density (kg m^{-3})
τ_a	Cold snow time constant for snow albedo aging (–)
τ_d	Seconds in one hour (3600 s h^{-1})
τ_h	Period of one day (86 400 s)
τ_f	Warm snow time constant for snow albedo aging (–)
τ_r	Time constant describing the snow density aging (–)
$a_{0,wd,we}$	Parameter defining the base Q_f per capita (W m^{-2} (capita^{-1} ha^{-1})$^{-1}$)
$a_{1,wd,we}$	Parameter related to CDD (W m^{-2} K^{-1} (capita^{-1} ha^{-1})$^{-1}$)
$a_{2,wd,we}$	Parameter related to HDD (W m^{-2} K^{-1} (capita^{-1} ha^{-1})$^{-1}$)
$a_{1,2,3}$	Constants in the calculation of the snow heat storage
a_r	Radiation melt factor (mm W^{-1} h^{-1})
a_t	Temperature melt factor (mm °C^{-1} h^{-1})
a_f	Temperature freezing factor (mm °C^{-1} h^{-1})
A	Study area (ha)
b	Empirical coefficient in the calculation of drainage
$b_{1,2,3}$	Parameters controlling the speed of leaf on
$b_{1a,2a,3a}$	Parameters for automatic irrigation (mm, mm K^{-1}, mm d^{-1})
$b_{1m,2m,3m}$	Parameters for manual irrigation (mm, mm K^{-1}, mm d^{-1})
Bldg	Building surface type
$c_{1,2,3}$	Parameter to control the speed of leaf-off
c_p	Heat capacity of air (J kg^{-1} K^{-1})
c_w	Specific heat capacity of water (kJ kg^{-1} °C^{-1})
C_i	Interception state of ith surface (mm)
$C_{soil,i}$	Soil water storage (mm)
C^R	Retention capacity (mm)
C^R_{min}	Minimum retention capacity (mm)
C^R_{max}	Maximum retention capacity (mm)
d	Day
$D_{0,i}$	Drainage rate (mm)

GMDD
7, 1063–1114, 2014

Table A1. Continued.

Decid	Deciduous surface type
E	Evaporation (mm h^{-1})
EC	Eddy covariance
Everg	Evergreen surface type
$f_{s,i}$	Fraction of snow on surface
$f_{s,i,0}$	Initial fraction of snow
F	Freezing water on surface (mm h^{-1})
$g_{i,\max}$	Maximum conductance (m s^{-1})
G_{1-6}	Parameters related to surface conductance
GDD	Growing degree days
i	Surface type index
Irr. veg.	Irrigated vegetation type
I	Interception of linear regression
I_w	Additional water to water surface type (mm)
$K\downarrow$	Downward shortwave radiation (W m^{-2})
$K\downarrow_m$	Maximum incoming solar radiation used in
g_s	calculation
$K\uparrow$	Upward shortwave radiation (W m^{-2})
K_s	Saturated hydraulic conductivity (mm s^{-1})
Ku	Kumpula site
Ku1	Built sector at the Kumpula site
Ku2	Road sector at the Kumpula site
Ku3	Vegetation sector at the Kumpula site
L_f	Latent heat of fusion (J kg^{-1})
$\mathrm{LAI}_{d,i}$	Daily leaf area index (m^2 m^{-2})
$\mathrm{LAI}_{\max,i}$	Maximum LAI of surface type i (m^2 m^{-2})
$\mathrm{LAI}_{\min,i}$	Maximum LAI of surface type i (m^2 m^{-2})
Lat	Latitude (°)
Lon	Longitude (°)
M	Snow melt and re-freezing of melted water (mm h^{-1})
MBE	Mean biased error
nRMSE	Normalized root mean square error
N	Number of data points
OHM	Objective hysteresis model
p	Population density inside the grid (capita ha^{-1})
P	Precipitation (mm h^{-1})
Pa	Pasila site
Pav	Paved surface type
Pi	Pihlajamäki site
Pr	Pierrefonds-Roxboro site
Q^*	Net all-wave radiation (W m^{-2})
Q_A	Advective heat flux (W m^{-2})
Q_E	Latent heat flux (W m^{-2})
Q_f	Anthropogenic heat flux (W m^{-2})
Q_g	Ground heat flux (W m^{-2})
Q_H	Sensible heat flux (W m^{-2})
Q_M	Energy consumed to melt snow (W m^{-2})
Q_p	Heat released from rain on snow (W m^{-2})
r	Perssons correlation coefficient
r_a	Aerodynamic resistance (s m^{-1})
$r_{s,\max}$	Maximum surface resistance (s m^{-1})
res_{cap}	Surface water capacity in LUMPS (mm)
res_{drain}	Drainage rate of water bucket in LUMPS (mm h^{-1})
R	Runoff (mm)
R_C	Limit when surface is totally covered with water in LUMPS (mm)
Rl	Rosemont–La-Petite-Patrie site
R_{mod}	Modelled runoff (mm)
R_{obs}	Observed runoff (mm)

Table A1. Continued.

RMSE	Root mean square error
s	Slope of the saturation vapour pressure curve over ice (Pa°C^{-1})
s_d	Snow depth (m)
S	Slope of linear regression
S_{1-2}	Parameters related to surface conductance
S_i	State of the snow free surface (mm)
S_{Pipe}	Maximum depth capacity of pipes (mm)
$S_{soil,i}$	Soil state (mm)
S_{WE}	Snow water equivalent (mm)
$S_{WE,0}$	Initial snow water equivalent (mm)
$S_{WE,Lim}$	Limit of the snow water equivalent for the snow removal (mm)
$S_{WE,i}^{max}$	Snow water equivalent when surface type
i	is fully covered with snow (mm)
SDD	Senescence degree days
SUEWS	the Surface Urban Energy and Water balance Scheme
t_d	Day length (h)
T_a	Air temperature (°C)
$T_{BaseGDD}$	Base temperature for leaf growth (°C)
$T_{BaseSDD}$	Base temperature for senescence (°C)
T_{BaseQF}	Base temperature for Q_F (°C)
T_H, T_L	Parameters related to calculation of g_s (°C)
T_{lim}	Temperature limit for the liquid precipitation and snow (°C)
T_s	Snow surface temperature (°C)
T_{Step}	Time step for water balance calculation(s)
T_R	Transport of snow from the study area (mm)
V	Vapour pressure deficit (Pa)
X_{Mod}	Modelled variable X
$X_{Mod,max}$	Maximum value of observed time series
X_{Obs}	Observed variable X
$X_{Obs,max}$	Maximum value of observed time series
z	Height of the meteorological measurements (m)
z_{0v}	Roughness length for heat and water vapour (m)
z_{0m}	Roughness length for momentum (m)
z_h	Mean building height (m)
z_t	Mean tree height (m)

GMDD
7, 1063–1114, 2014

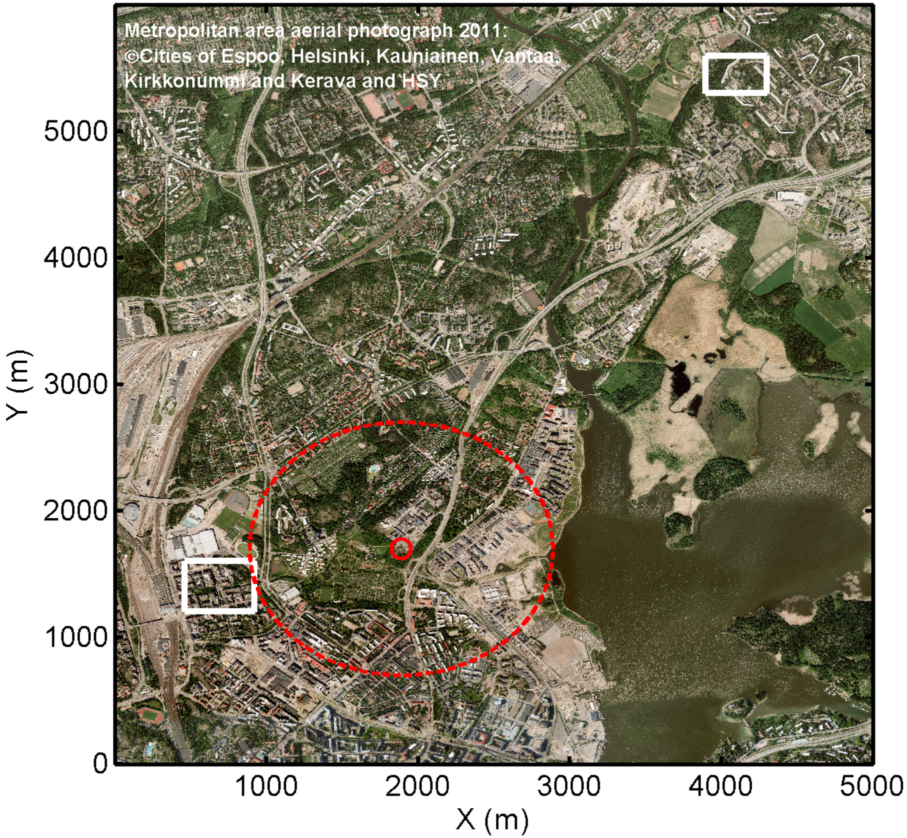

Fig. 1. Aerial photograph of the measurement locations in Helsinki. Red dot is the SMEARIII-Kumpula site (Ku). The red dashed line is the 1 km radius circle that the surface cover fractions are calculated for, and the white squares show the approximate locations of the catchment areas (Pa left side and Pi top-right).

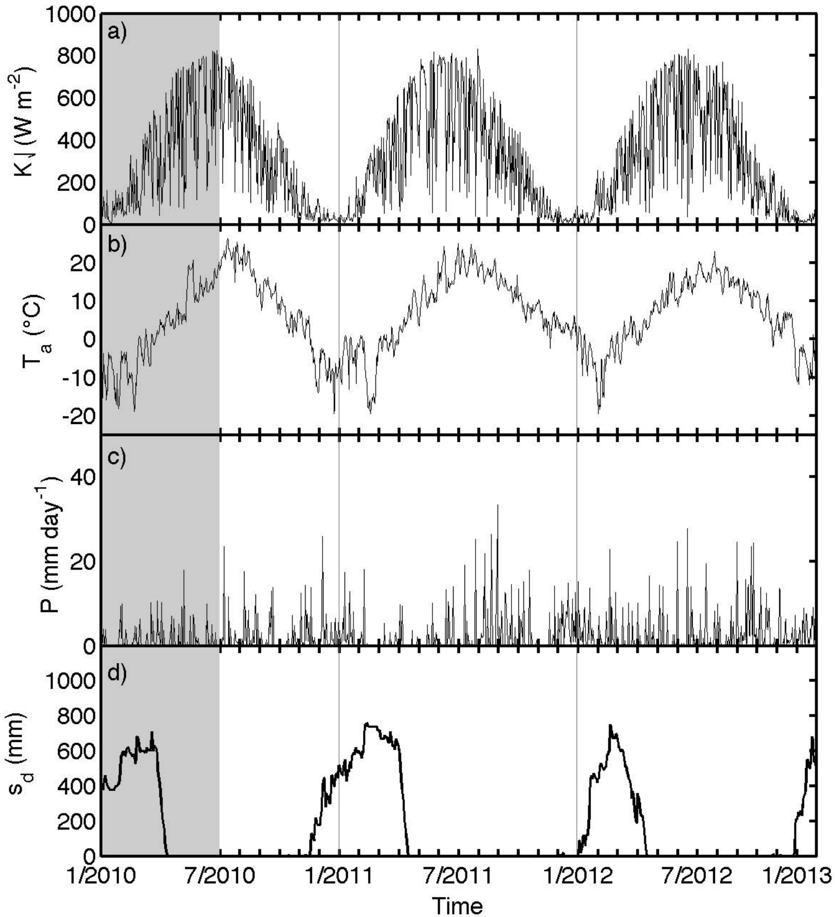

Fig. 2. Time series of daily **(a)** daytime (10:00–14:00) solar radiation ($K\downarrow$), **(b)** air temperature (T_a), **(c)**, precipitation (P) measured in SMEAR III – Kumpula, and **(d)** snow depth measured at Kumpula. Grey area shows the spin-up period.

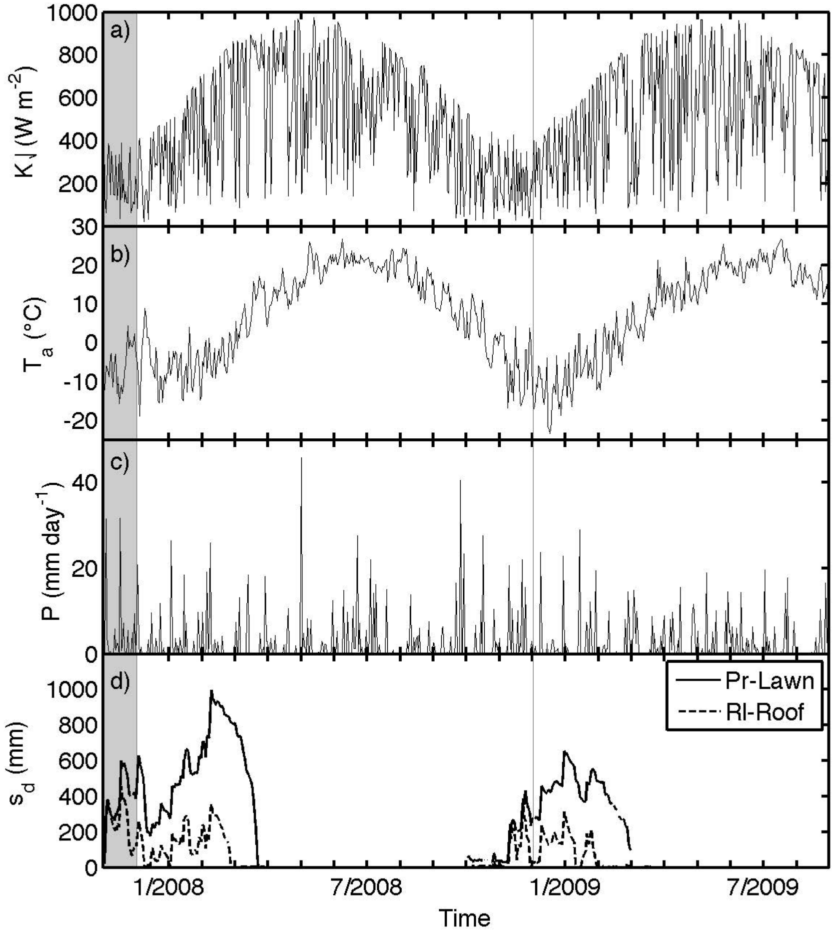

Fig. 3. As Fig. 2 but for Montreal measured at the suburban site (Pr) with snow depth measured in a suburban back lawn (Pr) and urban roof (Rl).

GMDD
7, 1063–1114, 2014

Development of the SUEWS for cold climate cities

L. Järvi et al.

Title Page
Abstract Introduction
Conclusions References
Tables Figures
Back Close
Full Screen / Esc
Printer-friendly Version
Interactive Discussion

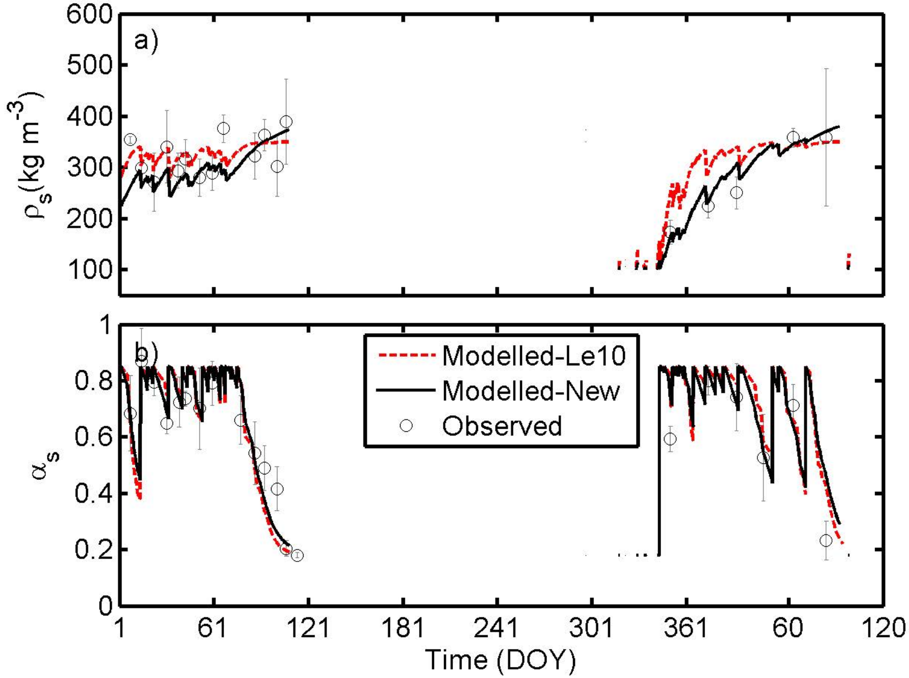

Fig. 4. Observed and modelled **(a)** snow density (ρ_s) and **(b)** snow albedo (α_s) at the suburban site in Montreal (January 2008–April 2009). Observed values are the medians from four locations and the error bars show the quartile deviations. Aging functions proposed in Lemonsu et al. (2010) "Le10" and in the current study ("New").

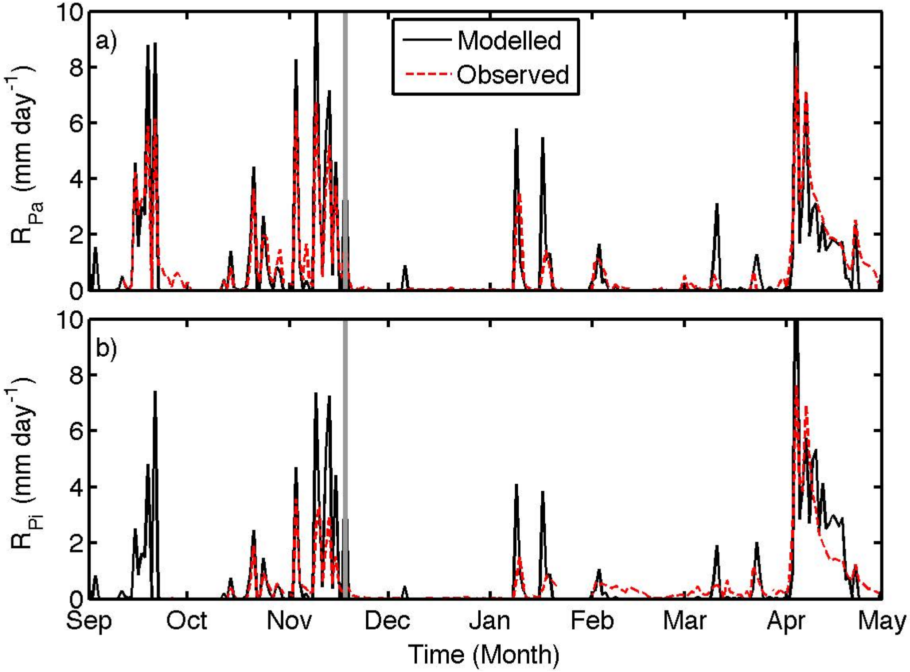

Fig. 5. Modelled and observed runoff at **(a)** Pa and **(b)** Pi (independent) sites. Grey line indicates when the snow starts to accumulate on ground; the snow melts by the end of April.

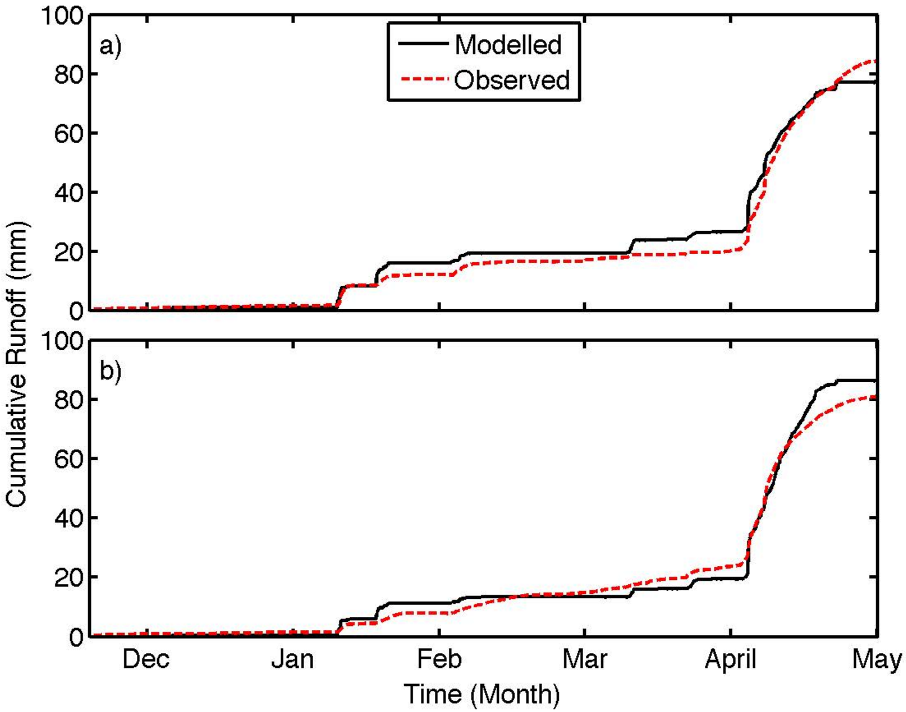

Fig. 6. Modelled and observed cumulative runoff during the snow covered period (19 November 2010–31 April 2011) **(a)** Pa and **(b)** Pi (independent) catchments.

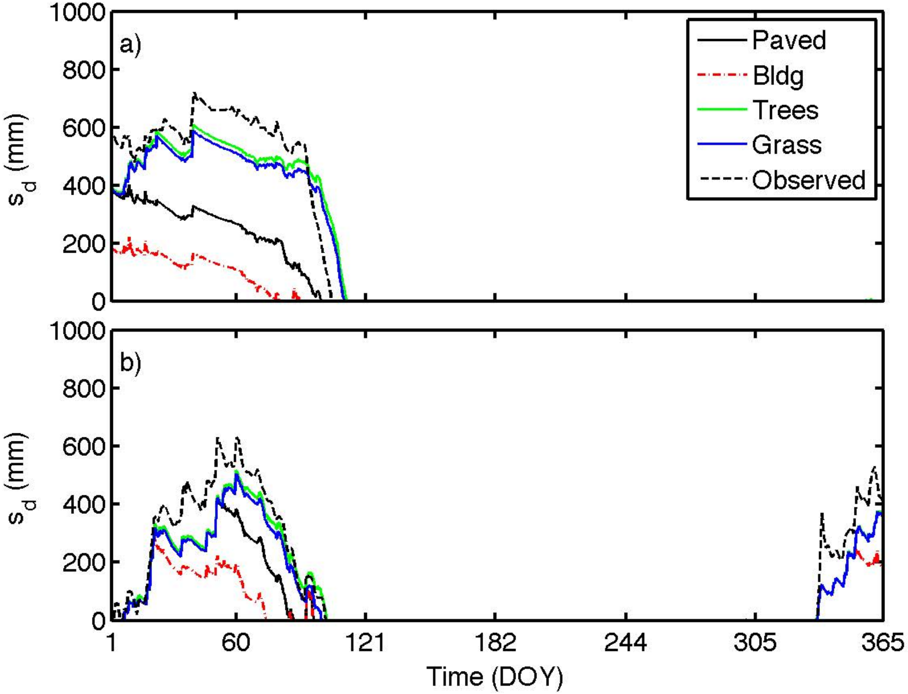

Fig. 7. Simulated (by surface type) and observed snow depth in Helsinki in **(a)** 2011 and **(b)** 2012.

GMDD
7, 1063–1114, 2014

Development of the SUEWS for cold climate cities

L. Järvi et al.

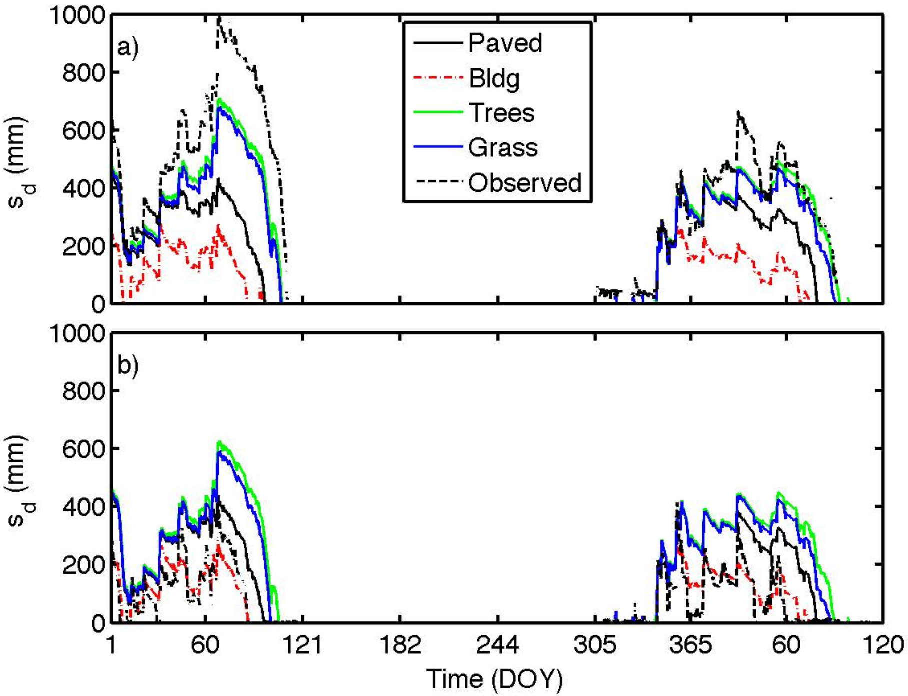

Fig. 8. As Fig. 7 for Montreal in 2008–2009 **(a)** suburban site with observations above (grass) lawn and **(b)** urban site with (building) roof observations.

GMDD
7, 1063–1114, 2014

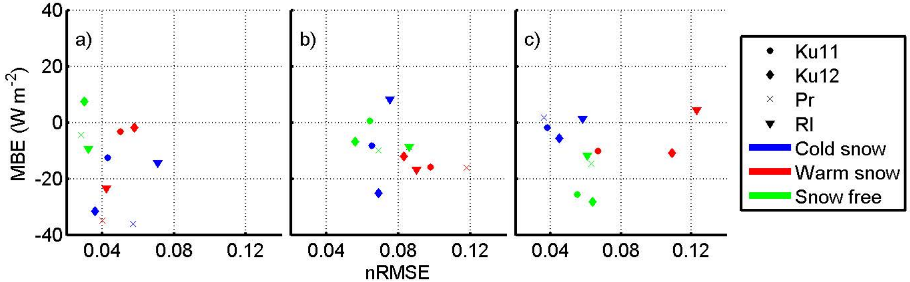

Fig. 9. Model performance for **(a)** net all-wave radiation (Q^*), **(b)** sensible heat (Q_H) and **(c)** latent heat flux (Q_E). Mean bias error (MBE) vs. normalized root mean square error (nRMSE) for different sites and for Ku separately (years 2011 (Ku11) and 2012 (Ku12)).

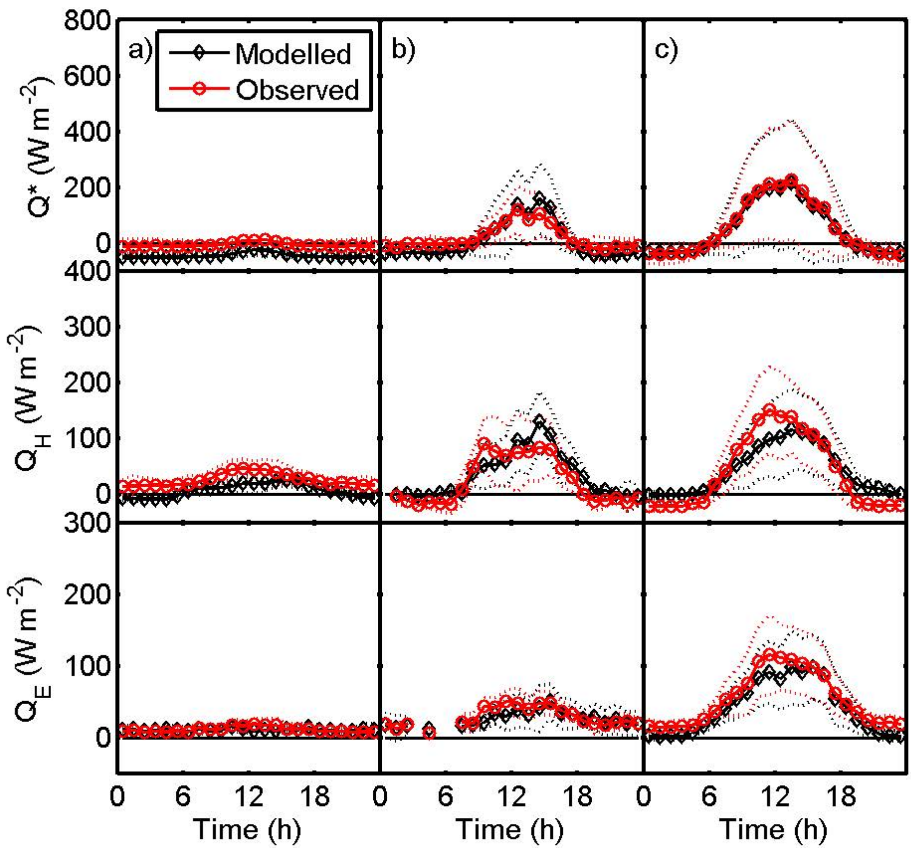

Fig. 10. Diurnal behaviour of the measured and modelled net all-wave radiation (Q^*) and turbulent energy fluxes (Q_H and Q_E) during **(a)** cold snow, **(b)** melting snow and **(c)** snow-free periods in Helsinki in 2012. Only hours when observations are available were used. Dotted lines show the quartile deviations.

GMDD
7, 1063–1114, 2014

Development of the SUEWS for cold climate cities

L. Järvi et al.

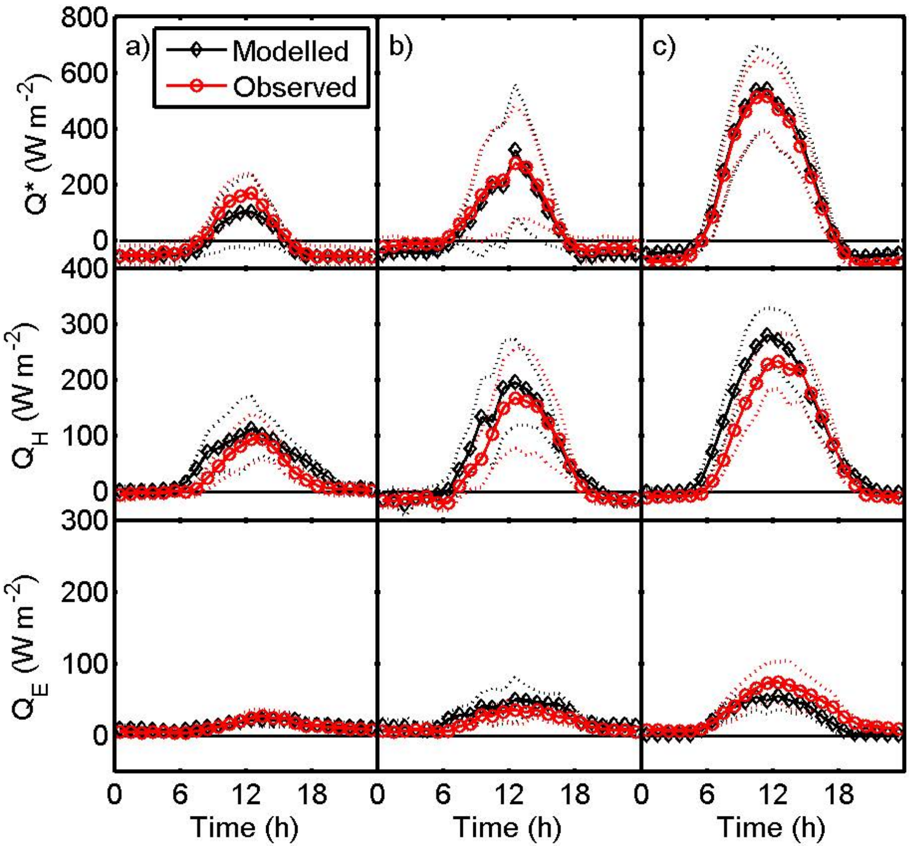

Fig. 11. As Fig. 10, for the urban site in Montreal (RI) in 2008–2009.

GMDD

7, 1063–1114, 2014

Development of the SUEWS for cold climate cities

L. Järvi et al.

Title Page
Abstract | Introduction
Conclusions | References
Tables | Figures
◂| |▸
◂ ▸
Back | Close
Full Screen / Esc
Printer-friendly Version
Interactive Discussion

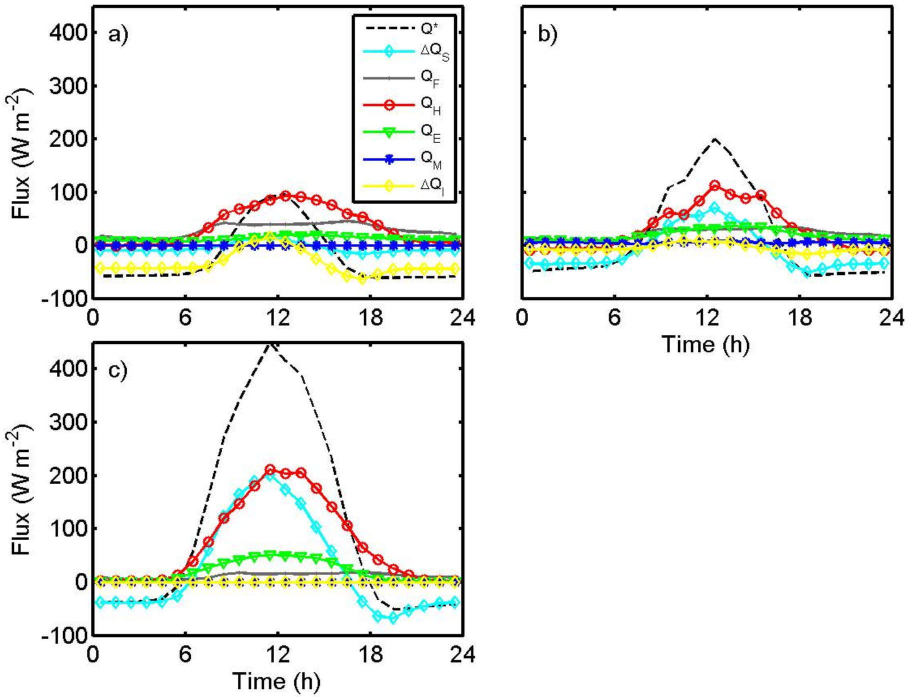

Fig. 12. Energy balance at the urban site (RI) in Montreal during **(a)** cold snow, **(b)** warm snow and **(c)** snow free periods. Q^* = net all wave radiation, ΔQ_S = heat storage to snow free surfaces, Q_F = anthropogenic heat flux, Q_H = sensible heat flux, Q_E = latent heat flux, Q_M = snow melt/freezing water related energy flux, and ΔQ_I = heat storage in snow pack.

GMDD
7, 1063–1114, 2014